

# Navigating Demand Uncertainty in Container Shipping: Deep Reinforcement Learning for Enabling Adaptive and Feasible Master Stowage Planning

Jaike van Twiller<sup>1</sup>, Yossiri Adulyasak<sup>2</sup>, Erick Delage<sup>2</sup>, Djordje Grbic<sup>1</sup>, Rune Møller Jensen<sup>1</sup>

<sup>1</sup>IT University of Copenhagen, <sup>2</sup>HEC Montréal

Corresponding author: jaiv@itu.dk

## Abstract

Reinforcement learning (RL) has shown promise in solving various combinatorial optimization problems. However, conventional RL faces challenges when dealing with complex, real-world constraints, especially when action space feasibility is explicit and dependent on the corresponding state or trajectory. In this work, we address stochastic sequential dynamic decision-making problems with state-dependent constraints. As a relevant and real-world case study, we focus on the master stowage planning problem in container shipping, which aims to optimize revenue and operational costs under demand uncertainty and operational constraints. We propose a deep RL framework with an encoder-decoder model and feasibility layers that satisfy convex constraints and maintain unbiased gradient flow, which embed problem instances, current solutions, and demand uncertainty to guide learning. Experiments show that our model efficiently finds adaptive, feasible solutions that generalize across varying distributions and scale to larger instances, outperforming state-of-the-art baselines in constrained RL and stochastic programming. By uniting artificial intelligence and operations research, our policy empowers humans to make adaptive, uncertainty-aware decisions for resilient and sustainable planning.

## Introduction

In recent years, machine learning (ML) for combinatorial optimization (CO) has gained significant traction, driving advances in solving complex decision problems (Bengio, Lodi, and Prouvost 2021). Learning advanced planning policies yields promising results in solving established problems, such as vehicle routing (Kool, van Hoof, and Welling 2019; Hottung, Kwon, and Tierney 2022) or job shop scheduling (Kwon et al. 2020). Although benchmarking algorithms on well-known problems is essential, much work on ML for CO focuses on simplified, deterministic, and static settings with implicit feasibility. In contrast, real-world problems are often stochastic, dynamic, and subject to explicit constraints dependent on states or trajectories. We address this challenge by bridging artificial intelligence (AI) and operations research for practical and impactful planning.

A relevant domain is container shipping, which transports 45% of global goods worth \$8.1 trillion annually (United

Nations Conference on Trade and Development 2021), emits over 200 million tonnes of CO<sub>2</sub> yearly (Lloyd's List 2022), yet remains key to the green transition due to its relatively low emissions per ton-mile (European Commission 2023). Container shipping has highly combinatorial, uncertain, and operationally constrained problems, i.e., berth allocation (Martin-Iradi, Pacino, and Ropke 2022), pre-marshalling (Hottung, Tanaka, and Tierney 2020), quay crane scheduling (Herup et al. 2022), and container vessel stowage planning (Van Twiller et al. 2024b). The latter can decompose into two persistently challenging subproblems: the master planning problem (MPP) assigns cargo to clusters of slots, and the slot planning problem (SPP) allocates containers to individual slots (Pacino et al. 2011). These problems involve stochastic, dynamic decisions subject to constraints, where actions affect future feasibility and poor decisions cause disruptions and unnecessary emissions in global supply chains.

This paper presents a deep reinforcement learning (DRL) framework with feasibility projection that learns to act in complex, uncertain environments while enforcing hard constraints. Conventional RL struggles with feasibility, while stochastic programs and implicit optimization incur high computational costs. Instead, our method efficiently learns from experience and corrects infeasible actions. We formulate the MPP under demand uncertainty as a Markov decision process (MDP) and solve it using a projected encoder-decoder model that integrates instance, solution, and uncertainty data. Differentiable projections with Jacobian corrections ensure unbiased gradient flow and enable stable training of feasible policies. Our main contributions are:

- **MPP Environment:** A novel stochastic, dynamic MDP with state-dependent constraints for the MPP under demand uncertainty to benchmark AI policies and address data scarcity in shipping. Released as open-source code<sup>1</sup>
- **Unbiased Violation Projection:** We propose differentiable feasibility projections that ensure satisfaction of general convex and problem-specific constraints, including unbiased gradient flow through Jacobian corrections.
- **Scalable and Adaptive Solutions:** Our model uniquely surpasses state-of-the-art constrained RL and stochastic MIP baselines by efficiently generating feasible, high-profit solutions that scale and adapt to varied instances.

<sup>1</sup><https://tinyurl.com/navigating-mpp-uncertainty>

- **Practical Decision Support:** We demonstrate how AI policies assist human planners in making uncertainty-aware decisions to address real-world challenges.

## Domain Preliminaries

We present some domain preliminaries to provide context. For a comprehensive review, we refer to Jensen et al. (2018).

**Voyages and Container Transport.** Liner shipping companies operate vessels on fixed-schedule, closed-loop voyages, much like a maritime bus service. These journeys, often exceeding ten ports, typically originate in supply-surplus regions (e.g., Asia) and finish in high-demand areas (e.g., Europe). A voyage can be described as a directed path graph  $G_P = (P, E_P)$ , where  $P = \{1, 2, \dots, N_P\}$  are the nodes representing ports, and  $E_P = \{(p, p+1) \mid p \in \{1, 2, \dots, N_P-1\}\}$  are the edges representing legs between ports. We define sub-voyages by the set  $P_{\text{start}}^{\text{end}} = \{p \in P \mid \text{start} \leq p \leq \text{end}\}$ . Containers have a port of load ( $pol$ ) and a port of discharge ( $pod$ ), also named transports or origin-destination pairs. A transport  $tr = (pol, pod)$  is defined with  $pol \in P_1^{N_P-1}$  and  $pod \in P_2^{N_P}$ . The set of all possible transports is  $TR = \{(i, j) \in P^2 \mid i < j\}$ .

**Container Cargo.** Container cargo is categorized by key characteristics: lengths (20 ft, 40 ft), weight classes (light, medium, heavy), and customer contracts (long-term, spot market) that determine cargo revenue ( $rev$ ). Long-term contracts offer lower but stable revenue and high volumes, taking priority over spot market contracts, which provide higher yet volatile revenue in lower volumes. The lack of no-show fees creates uncertainty in container demand, although this becomes more predictable closer to the arrival date. This necessitates dynamic cargo allocation to vessels during the voyage. Containers are often grouped into cargo classes by characteristics, such as  $K = \{20\text{ft}, 40\text{ft}\} \times \{\text{Light, Medium, Heavy}\} \times \{\text{Spot, Long}\}$ .

**Vessel Layout.** Figure 1 shows the cellular layout of container vessels with standardized coordinates of ( $bay$ ,  $row$ ,  $tier$ ). It is divided into bays (02-38) ranging from the front (e.g., bay 02) to the rear (e.g., bay 38), also named from fore to aft. Bays are defined by an ordered set  $B = \{1, 2, \dots, N_B\}$ , ranging from fore to aft with  $N_B$  being the last bay. Each bay contains stacks of cells, whereas cells contain two slots that can hold two 20-foot containers or one 40-foot container. Bays are horizontally separated by hatch covers into above and below deck sections, introducing the set of decks  $D = \{d^{\text{above}}, d^{\text{below}}\}$ . It is worth noting that hatch covers introduce complexity since below-deck cargo can only be discharged if the above-deck cargo is cleared.

**Utilization.** Vessel utilization  $u_p \in \mathbb{Z}_{\geq 0}^{|B| \times |D| \times |K| \times |TR|}$  represents the cargo placement across bays  $B$ , decks  $D$ , cargo types  $K$ , and transports  $TR$ . Load operations are defined by  $u_p^+ \in \mathbb{Z}_{>0}^{|B| \times |D| \times |K| \times |TR|}$ , whereas discharging is denoted by  $u_p^- \in \mathbb{Z}_{>0}^{|B| \times |D| \times |K| \times |TR|}$ . The utilization at port  $p$  is defined as  $u_p = u_{p-1} + u_p^+ - u_p^- \forall p \in P$ , where  $u_0$  is

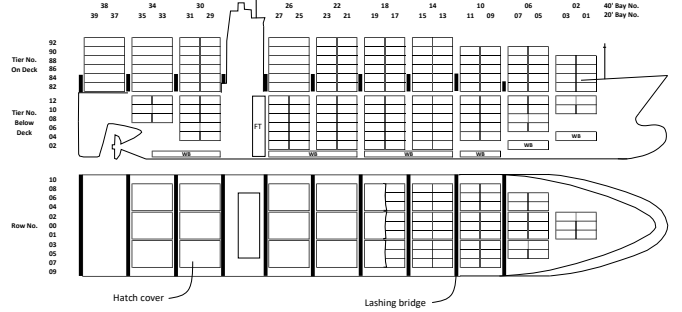


Figure 1: The side and top view of a container vessel.

the vessel's arrival condition at the first port. We also define the vessel's pre-loading utilization  $u'_p = u_{p-1} - u_p^-$ .

**Objectives and Global Constraints.** The MPP creates a capacity management plan for each general location (bay, deck) to maximize revenue and minimize costs, while the subsequent SPP assigns containers to specific slots. Due to multi-port voyages, each decision affects future feasibility and optimality. Due to frequent re-planning, runtimes over 10 minutes are impractical (Pacino et al. 2011).

Key efficiency objectives include minimizing over-stowage (an NP-hard problem (Tierney, Pacino, and Jensen 2014)) and crane makespan. Overstowage occurs when containers block access to those below needing discharge, requiring unnecessary moves. Minimizing makespan reduces port stay duration and associated costs.

Furthermore, vessels must satisfy safety constraints for seaworthiness, particularly their weight distribution. The longitudinal (lcg) and vertical (vcg) centers of gravity for load  $u_p$  must remain within bounds, where  $\otimes$  denotes outer product and  $\odot$  element-wise product:

$$\underline{lcg} \leq \frac{\mathbf{1}^\top (lm \odot u_p)}{\mathbf{1}^\top (w \odot u_p)} \leq \overline{lcg}, \quad \forall p \in P \quad (1)$$

$$\underline{vcg} \leq \frac{\mathbf{1}^\top (vm \odot u_p)}{\mathbf{1}^\top (w \odot u_p)} \leq \overline{vcg}, \quad \forall p \in P \quad (2)$$

where  $lm = ld \otimes w$  and  $vm = vd \otimes w$  are longitudinal and vertical moments, with  $w \in \mathbb{R}_{>0}^{|K| \times |TR|}$  being container weights, and  $ld, vd \in \mathbb{R}^{|B| \times |D|}$  denoting the respective longitudinal and vertical distances from the center of gravity.

The problem's scale and complexity, combined with data scarcity and runtime limits, make most models focus on constraint subsets for tractability. This highlights the need for efficient AI-driven solutions to enhance decision support.

## Related Work

Various solution methods have been proposed to address container stowage planning, including exact algorithms (Roberti and Pacino 2018), relaxed MIPs (Pacino et al. 2011), matheuristics (Parreño-Torres et al. 2021), meta-heuristics (Chang, Hamed, and Haghani 2022; Pacino 2018), and hybrid frameworks (Bilican, Evren, and Karatas

2020). A recent survey highlights that scalable solutions for representative stowage planning and the MPP remain unsolved (Van Twiller et al. 2024b). Crucially, most research assumes deterministic problems with cost minimization, overlooking real-world needs for profit maximization in the face of demand uncertainty. Our work targets this gap by optimizing the MPP under demand uncertainty.

**Stochastic Programming.** Traditionally, uncertainty in optimization is handled using stochastic programming (Birge and Louveaux 2011). It models discrete scenarios over multiple stages, forming a scenario tree with exponential complexity  $\mathcal{O}(b^T)$ , where  $b$  is the branching factor and  $T$  the number of stages. Consequently, multi-stage problems with  $T > 2$  and a reasonably large  $b$  are often intractable. Common mitigations include scenario reduction (Römisch 2009), Benders or Lagrangian decomposition (Rahmaniani et al. 2017), and progressive hedging to enforce non-anticipativity iteratively (Boland et al. 2018). Alternatively, approximation methods improve tractability: stochastic dual dynamic programming applies temporal decomposition but depends on known uncertainty distributions (Shapiro 2011), while sample average approximation uses Monte Carlo sampling to solve a deterministic surrogate (Chen and Luedtke 2022). Model-free RL bypasses most of the mentioned drawbacks by learning policies through direct interaction, implicitly modeling uncertainty for dynamic environments (Powell 2022). However, it faces challenges in sample efficiency and handling complex constraints.

**Learning with Hard Constraints.** Enforcing constraints in differentiable models is challenging because it requires balancing feasibility and objectives. Soft feasibility regularization, such as penalty functions (Zhang et al. 2022), barrier methods (Wang et al. 2023), or primal-dual algorithms (Ding et al. 2020), lacks strict guarantees and needs careful tuning. Decoupled methods, e.g., post-hoc repair or safety shields (Alshiekh et al. 2018), ensure feasibility but sacrifice differentiability, limiting end-to-end learning. Integrated techniques, like differentiable implicit optimization (Agrawal et al. 2019) or differentiable projection layers (Donti, Rolnick, and Kolter 2021; Chen, Tanneau, and Van Hentenryck 2024), embed constraints directly but produce biased gradients and computational overhead. Our work introduces a differentiable violation projection that enforces hard convex constraints and ensures unbiased gradients via Jacobian correction, enabling efficient learning in constrained problems.

## Markov Decision Processes

We formulate the MPP as an MDP with action constraints. Intuitively, the MDP tracks what's loaded and needed at each port (state), chooses how to load (action), updates the vessel and demand per port (transition), and measures profit after every decision (reward). To improve learning efficiency, we decompose the MDP into a sequence of simpler decisions, thereby effectively reducing the action space.

### Markov Decision Process

Let  $\mathcal{M} = (S, X, \mathcal{T}, \mathcal{R}, P_1^{N_P-1}, \gamma)$  define an episodic discounted MDP representing the MPP, where  $S$  is a set of

states,  $X$  is a set of actions,  $\mathcal{T} : S \times X \rightarrow \Delta(S)$  is the transition function,  $\mathcal{R} : S \times X \times P_1^{N_P-1} \rightarrow \mathbb{R}$  is the reward function,  $P_1^{N_P-1}$  is the finite horizon of load ports with last port  $N_P - 1$ , and  $\gamma \in (0, 1)$  is the discounting factor.

**State.** The state  $s_p = (u_p, q_p, \zeta)$  includes vessel utilization  $u_p \in \mathbb{R}_{\geq 0}^{n_u}$ , realized demand  $q_p \in \mathbb{R}_{\geq 0}^{n_q}$ , and instance parameter  $\zeta$  (such as demand statistics, port and cargo indices, TEU, weight, revenue; details in Appendix ). The initial state  $s_0 = (u_0, q_0, \zeta)$  has an empty vessel  $u_0 = \mathbf{0}^{n_u}$ , realized demand  $q_0$  of first port, and a generated problem instance  $\zeta$ . Note that  $n_u = |B| \times |D| \times |K| \times |TR|$ ,  $n_c = |B| \times |D|$  and  $n_q = |K| \times |TR|$  are the shapes of utilization, location and demand, respectively.

**Action.** At each port  $p$ , an action  $x_p \in \mathbb{R}_{\geq 0}^{n_u}$  specifies how many containers of each group to load at each vessel position. To ensure safe and efficient loading, actions must satisfy a set of linear constraints defined by the polyhedron  $PH(s_p) = \left\{ x_p \in \mathbb{R}_{\geq 0}^{n_u} : A(s_p)x_p \leq b(s_p) \right\}$ , where  $A(s_p) \in \mathbb{R}^{m_u \times n_u}$  is the constraint matrix and  $b(s_p) \in \mathbb{R}^{m_u}$  is the vector of bounds, with  $m_u$  different constraints.

The constraints below are expressed in terms of the action  $x_p$  and the pre-loading utilization  $u'_p$ , meaning the vessel's state after discharging cargo at the port. We use real-valued actions, as downstream planning stages (e.g., the SPP) will discretize these plans (Pacino et al. 2011).

Constraint (3) limits load  $x_p$  to the available demand  $q_p$ , while Constraint (4) ensures  $x_p$  does not exceed the residual TEU capacity. Constraints (5)–(6) enforce lcg limits, while Constraints (7)–(8) impose similar bounds on the vcg. These stability bounds are derived from Constraints (1) and (2). Full derivations of  $PH(s_p)$  are provided in Appendix .

$$x_p^\top \mathbf{1}_{n_c} \leq q_p \quad (3)$$

$$x_p^\top \mathbf{teu} \leq c - u'_p \mathbf{teu} \quad (4)$$

$$-\mathbf{1}^\top ((lm - \underline{lcgw}) \odot x_p) \leq -\mathbf{1}^\top ((\underline{lcgw} - lm) \odot u'_p) \quad (5)$$

$$\mathbf{1}^\top ((lm - \overline{lcgw}) \odot x_p) \leq \mathbf{1}^\top ((\overline{lcgw} - lm) \odot u'_p) \quad (6)$$

$$-\mathbf{1}^\top ((vm - \underline{vcgw}) \odot x_p) \leq -\mathbf{1}^\top ((\underline{vcgw} - vm) \odot u'_p) \quad (7)$$

$$\mathbf{1}^\top ((vm - \overline{vcgw}) \odot x_p) \leq \mathbf{1}^\top ((\overline{vcgw} - vm) \odot u'_p) \quad (8)$$

**Transition.** We use a stochastic transition function  $\mathcal{T}(s_{p+1} | s_p, x_p)$  to update the state at each port. Each step of the transition, when moving to port  $p + 1$ , includes:

- Upon port arrival, the true demand  $q_{p+1}$  is revealed, while future port demand remains unknown.
- Cargo destined for this port is unloaded:  $u_{p+1} = u_p \odot (1 - \mathbf{e}_p^-)$ , with  $\mathbf{e}_p^-$  marking which cargo to discharge.
- New cargo is loaded:  $u_{p+1} = u_{p+1} + x_p$ , where action  $x_p$  should fit feasible region  $PH(s_p)$ .

**Reward.** Equation (9) defines a deterministic reward function that computes profit as revenue minus costs. Revenue is calculated as the sum of loaded containers  $x_p$  that match actual demand  $q_p$ ; no revenue is received for containers exceeding demand. Costs are determined using

two state-dependent auxiliary variables: hatch overstows  $ho(s_p, p) \in \mathbb{R}_{>0}^{|B|}$  and excess crane moves  $cm(s_p, p) \in \mathbb{R}_{>0}^{|B|-1}$ . Both components are weighted, respectively, by coefficients  $ct^{ho} \in \mathbb{R}_{>0}$  and  $ct^{cm} \in \mathbb{R}_{>0}$ .

$$\begin{aligned}\mathcal{R}(s, x, p) = & \text{rev min} (x^\top \mathbf{1}_{n_c}, q) \\ & - ct^{ho} \mathbf{1}^\top ho(s, p) + ct^{cm} \mathbf{1}^\top cm(s, p).\end{aligned}\quad (9)$$

## Decomposed Markov Decision Process

The MDP has an action space of size  $|X| \propto |B| \cdot |D| \cdot |K| \cdot |P|$ , where each action  $x_p$  determines how cargo types and transport options are placed on the vessel per port. However, this action space is large, which can hinder learning efficiency (Kanervisto, Scheller, and Hautamäki 2020).

To address this, we decompose the MDP into granular, sequential steps based on an index  $(i, j, k) \forall (i, j) \in TR, k \in K$ . Figure 2 illustrates the decomposed MDP for a single port. Instead of placing all transport and cargo types simultaneously, we take a decomposed action for all transports  $(p, j)$  and cargo types  $k$  at port  $p$ , then departing to a new port. This reduces the action space to  $|X| = |B| \cdot |D|$ , while unfolding transports and cargo types over an extended time horizon  $t \in H = \{0, 1, \dots, T_{\text{seq}}\}$  with  $T_{\text{seq}} = |K| \cdot |TR|$ .

**State.** The state  $s_t = (u_t, q_t, \zeta)$  depends on time step  $t$ , where  $u_t \in \mathbb{R}_{\geq 0}^{n_u}$  is vessel utilization, and  $q_t \in \mathbb{R}_{\geq 0}^{n_q}$  is realized demand. The instance  $\zeta$  remains unchanged. Given the time  $t$ , however, we can extract relevant parameters from  $\zeta$ , such as  $(pol_t, pol_t, k_t)$ ,  $rev^{(pol_t, pol_t, k_t)}$ .

**Action.** Action  $x_t \in \mathbb{R}_{\geq 0}^{n_c}$  assigns real number of containers to utilization  $u_t$  for step  $t$ . Each action is subject to  $PH(s_t) = \{x_t \in \mathbb{R}_{>0}^{n_c} : A(s_t)x_t \leq b(s_t)\}$ . Here,  $A(s_t) \in \mathbb{R}^{m_c \times n_c}$  is the constraint matrix,  $b(s_t) \in \mathbb{R}^{m_c}$  is the bound vector, and  $m_c$  is the number of constraints. It is also worth noting that Constraints (3)-(8) are reformulated to fit feasible region  $PH(s_t)$ .

**Transition.** At each time  $t$ , the transition includes loading, where  $x_t$  is added to  $u_t$ . Discharges and demand realizations occur when arriving at a new port, indicated by  $t \in T_{\text{new port}}$ .

**Reward.** The revenue at step  $t$  is computed as  $rev(pol_t, pod_t, k_t) \min(1^\top x_t, q_t^{(pol_t, pod_t, k_t)})$ . However, costs depend on knowing all loading operations at port  $p$ , which is aggregated in utilization  $u_t$  at the last step of the port  $t \in T_{\text{leave port}}$ . As a result, the cost signal is sparse, being evaluated only once per port  $p$ , rather than at each step.

## Proposed Architecture

Figure 3 shows our projected encoder-decoder model, which embeds instance, context, and dynamic data to obtain a stochastic look-ahead policy  $\pi_\theta(x|s_t)$  parameterized by mean  $\mu_\theta(s_t)$  and standard deviation  $\sigma_\theta(s_t)$ . The policy output is projected by layer  $\mathcal{P}$  to ensure feasibility, and adjusted actions are used in the decomposed MDP. We train the projected policy with actor-critic RL, learning to interact in the decomposed MDP with a critic evaluating actions.

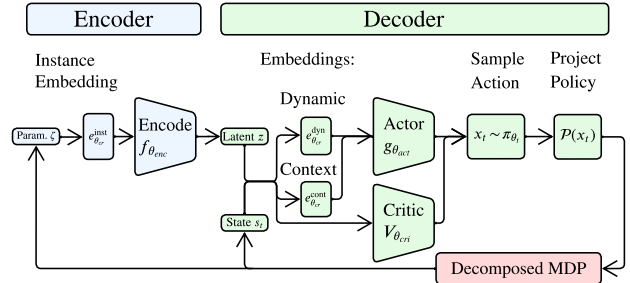


Figure 3: Deep reinforcement learning architecture with feasibility projection for actor-critic methods.

## Encoder-Decoder Model

Our model, adapted from Kool, van Hoof, and Welling (2019) and extended with a critic, is illustrated in Figure 4.

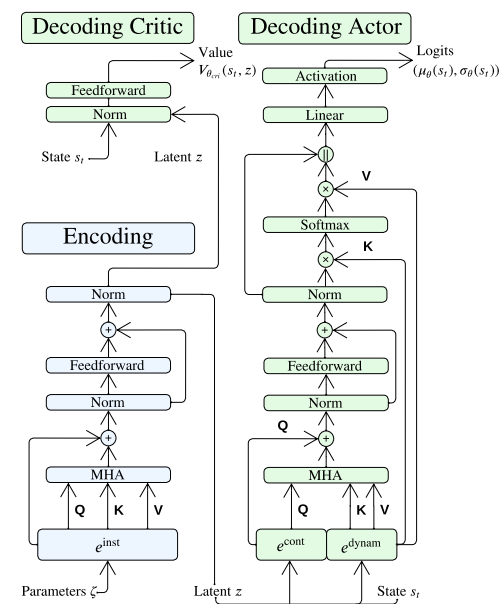


Figure 4: Layers of the encoder and the actor-critic decoder

**Instance Embedding.** The embedding  $e^{\text{inst}}(\zeta)$ , parameterized by  $\theta_{cr}$ , maps problem instance  $\zeta$  to a feature representation used by the encoder to condition policies on instances. Sinusoidal positional encoding is then applied to inform the model of element order in sequences (Vaswani et al. 2017).

**Encoding Layers.** An attention encoder  $f(e^{\text{inst}}(\zeta))$  parameterized by  $\theta_{\text{enc}}$  maps embedding  $e^{\text{inst}}(\zeta)$  to latent variable  $z$  using multi-head attention (MHA) to identify relevant features dynamically and handle variable input size (Vaswani et al. 2017). Then, we use a feed-forward network (FFN) with ReLU activation, layer normalization, residual connections, and dropout.

**Context Embedding.** The embedding  $e^{\text{cont}}(u_t, z)$ , parameterized by  $\theta_{co}$ , extracts features from the current solution  $u_t$  and the latent variable  $z$ . This embedding provides the MHA

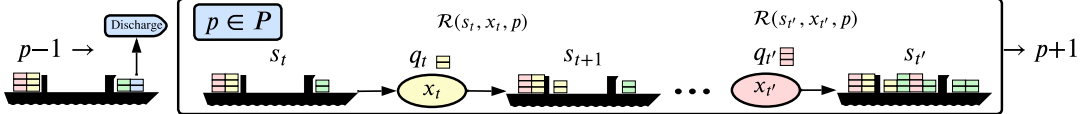


Figure 2: Illustration of the decomposed MDP for MPP. At port  $p$ , the vessel discharges cargo, observes realized demand  $q_t$ , then sequentially loads container type-POD pairs before sailing to the next port  $p+1$ . Colors indicate PODs.

query, helping the attention mechanism focus on relevant information, with the solution context at time  $t$ , enabling the policy to make informed decisions on the present state.

**Dynamic Embedding.** The embedding  $e^{\text{dyn}}(q_t, z)$ , parameterized by  $\theta_{\text{dn}}$ , extracts features from demand  $q_t$  across all time steps in the horizon  $H$ , capturing temporal patterns over the episode. By combining actual demand with latent information, it enables the attention mechanism to select (key) and retrieve (value) demand-related information over time for anticipating future conditions and long-term decision-making.

**Actor Layers.** Following (Kool, van Hoof, and Welling 2019), the actor decoder  $g(e^{\text{cont}}(u_t, z), e^{\text{dyn}}(q_t, z))$  is an attention model (AM) parameterized by  $\theta_{\text{act}}$ . The MHA layer uses context embedding as queries and dynamic embedding as keys and values encoding demand across the horizon, with a forward-looking mask on steps  $\{t, t+1, \dots, T_{\text{seq}}\}$  to link present context with future trends. An FFN extracts features, a pointer mechanism selects relevant future steps (Vinyals, Fortunato, and Jaitly 2015), and softplus activation then outputs positive logits  $(\mu_{\theta}(s_t), \sigma_{\theta}(s_t))$ .

**Critic Layers.** Our critic model  $V(s_t, z)$ , parameterized by  $\theta_{\text{cri}}$ , estimates the value of state  $s_t$  and latent variable  $z$  through an FFN outputting  $V_{\theta_{\text{cri}}}(s_t, z) \in \mathbb{R}$ .

**Action Policy.** The actor logits parameterize a stochastic Gaussian policy  $\pi_{\theta}(x|s_t) = \mathcal{N}((\mu_{\theta}(s_t), \sigma_{\theta}(s_t))$ , which allows action sampling  $x_t \sim \pi_{\theta}(x|s_t)$  to construct solutions.

### Feasibility Regularization in Actor-Critic Loss

Actor-critic methods such as proximal policy optimization (PPO) (Schulman et al. 2017) and soft actor critic (SAC) (Haarnoja et al. 2018) are widely used in unconstrained problems with implicitly encoded feasibility. A common approach to handle explicit action constraints is to augment the actor loss with a soft penalty term, known as feasibility regularization (FR) (Ding et al. 2020; Calvo-Fullana et al. 2021).

The actor loss is then defined as:

$$\mathcal{L}(\theta) = -\mathcal{L}_{\text{actor}}(\theta) + \lambda_f \mathcal{L}_{\text{feas}}(\theta) \quad (10)$$

$$\mathcal{L}_{\text{feas}}(\theta) = \mathbb{E}_t \left[ (A(s_t)x_{\theta}(s_t) - b(s_t))_{>0} \right] \quad (11)$$

where  $(\cdot)_{>0}$  denotes the ReLU function applied element-wise, penalizing only constraint violations, and  $\lambda_f$  controls the strength of regularization. For algorithms that do not propagate gradients through the action (e.g., PPO), we substitute  $x_{\theta}(s_t)$  with the policy mean  $\mu_{\theta}(s_t)$ .

However, tuning Lagrangian multipliers ( $\lambda_f$ ) is challenging, especially with constraints of varying scales, even in

static feasible regions. The problem worsens in dynamic, state-dependent regions  $PH(s_t)$  (Calvo-Fullana et al. 2021; Donti, Rolnick, and Kolter 2021), where the balance between reward and feasibility shifts over time. Thus, FR is often limited in such settings, though it remains a useful baseline due to its simplicity and broad adoption.

### Feasibility Projection Layers

To improve over FR, we incorporate differentiable projection layers that project sampled actions  $x_t$  before use in the decomposed MDP and policy update. These layers guarantee feasible actions and maintain gradient flow by correcting non-linear density changes via Jacobian adjustments to policy log-probabilities (Bishop 2006). Existing differentiable convex optimization layers (Agrawal et al. 2019) use implicit maps with intractable Jacobians, leading to biased gradients that hurt learning accuracy and high computational cost that limits efficiency. In contrast, we design unbiased projections with tractable Jacobians that enable corrections of log-probabilities, including one general convex layer and two constraint-specific variants. Details are in Appendix .

**Unbiased Violation Projection.** Algorithm 1 introduces the unbiased violation projection layer (UVP), which iteratively moves a sampled action  $x$  closer to the feasible set defined by a convex polyhedron  $PH = \{x \in \mathbb{R}_{>0}^n : Ax \leq b\}$ , where  $A \in \mathbb{R}^{m \times n}$  and  $b \in \mathbb{R}^m$ . Rather than enforcing strict feasibility at each step, UVP minimizes total constraint violation using gradient descent on the violation norm  $\|\mathcal{V}(x)\|_2^2$ , where  $\mathcal{V}(x) = (Ax - b)_{>0}$  which measures element-wise violations of constraints (Boyd and Vandenberghe 2004). Equation (12) provides the update rule with step size  $\eta_v$ , as implemented in Algorithm 1.

$$x' = x - \eta_v \nabla_x \|\mathcal{V}(x)\|_2^2 \quad (12)$$

As shown in Appendix , UVP iteratively reduces constraint violations without requiring exact feasibility, converging to a point of minimal violation and improving feasibility likelihood. During training, it runs for a fixed number of epochs; at inference, it stops when the change in total violation falls below  $\delta_v$ . Although UVP alters actions, we show in Appendix that it supports accurate learning by applying Jacobian-based log-probability corrections to account for the volume change induced by the transformation. This ensures distributional unbiasedness, i.e., the expected gradient after projection matches that before projection, which is crucial for correct and reliable learning with projection.

**Weighted Scaling Projection.** Function (13) defines the weighted scaling layer (WS), which normalizes vector  $x$  if

Algorithm 1: Unbiased violation projection layer

---

**Require:**  $x \in \mathbb{R}_{>0}^n$ , parameters  $(A, b, \eta_v, \delta_v)$

- 1: Initialize  $x' \leftarrow x$
- 2: Define  $\mathcal{V}(x) \leftarrow (Ax - b)_{>0}$
- 3: **for**  $i = 1$  **to** epochs **do**
- 4:   Set  $x \leftarrow x'$
- 5:   Update  $x' \leftarrow x - \eta_v A^\top \mathcal{V}(x)$
- 6:   **if**  $\mathbf{1}^\top \mathcal{V}(x') - \mathbf{1}^\top \mathcal{V}(x) \leq \delta_v$  **then**
- 7:     **break**
- 8:   **end if**
- 9: **end for**
- 10: **return**  $x'$

---

the sum of  $x$  exceeds scalar  $y$ . This preserves relative proportions of elements in  $x$  while enforcing  $\mathbf{1}^\top x = y$ .

$$\mathcal{W}(x, y) = \begin{cases} y \frac{\mathbf{1}^\top x}{\mathbf{1}^\top x} & \text{if } \mathbf{1}^\top x > y \\ x & \text{otherwise} \end{cases} \quad (13)$$

**Policy Clipping.** We can apply function  $\mathcal{C}(x, lb_{pc}, ub_{pc}) = \max(\min(x, ub_{pc}), lb_{pc})$  to enforce element-wise limits on vector  $x$ , thereby performing policy clipping (PC) on actions. However, PC is only applicable to box constraints.

## Experimental Results

We compare across data distributions on objective value (Obj.), training and test time (Time), and percentage of feasible instances (Feas.). An ablation study analyzes feasibility methods and gradient flow from actions, while managerial insights examine information value, computational cost, adaptiveness to uncertainty, and scaling to longer voyages.

## Experimental Setup

**Instances.** Training instances are Gaussian samples from  $\mathcal{N}(\mu^{(i,j,k)}, \sigma^{(i,j,k)}) \forall (i,j) \in TR, k \in K$ , with a randomized  $\mu^{(i,j,k)}$  and spread  $\sigma^{(i,j,k)} = CV\mu^{(i,j,k)}$  controlled by coefficient of variation CV. Generalization instances are continuous uniform samples from  $\mathcal{U}(lb^{(i,j,k)}, ub^{(i,j,k)}) \forall (i,j) \in TR, k \in K$ . Details are found in Appendix .

**Feasibility Mechanisms.** Table 1 summarizes the feasibility mechanisms. Feasibility regularization (FR) uses a static composite loss, while primal-dual methods (PD) learn  $\lambda_f$  for the same composite loss. AM with projection (AM-P) includes general (violation projection (UVP), convex program (CP) by Agrawal et al. (2019)), and constraint-specific layers (weighted scaling (WS), policy clipping (PC)). UVP, WS, and PC are evaluated standalone, but also with FR during training, and with CP-based inference.

**Runs and Baselines.** Offline training (4-port, 1000 TEU vessel) was conducted on an NVIDIA RTX A6000 GPU. Baselines span two categories: solving implicit stochastic environments (AM with FR or PD, AM-P with CP) and solving explicit scenario trees, (stochastic MIP without anticipation (SMIP-NA) and with perfect foresight (SMIP-PI) as an upper bound). SMIPs ran on an AMD EPYC 9454 48-core CPU. Implementation details are in Appendix and .

Type	Implementation	Constraints
FR/PD	Composite loss	Entire $PH(s_t)$
UVP	$UVP(x_t, A(s_t), b(s_t), \alpha_v, \delta_v)$	Entire $PH(s_t)$
CP	$CP(x_t, A(s_t), b(s_t))$ (inf.)	Entire $PH(s_t)$
WS	$\mathcal{W}(x_t, q_t)$	Demand $q_t$
PC	$\mathcal{C}(x_t, 0, c - u_t' teu)$	Capacity $c$

Table 1: Feasibility mechanisms and relation to constraints

## Policy Performance

Table 2 compares the performance of different methods. AM-P outperforms SMIP-NA with 30–40% higher objective profits and over 2 hours faster test time computation. AM with FR or PD shows inflated profits due to infeasible solutions; Appendix confirms that feasibility recovery ensures profits of \$1,200 and lower. In contrast, AM-P mostly finds feasible solutions with higher profits, highlighting FR and PD’s limitations. Among feasibility methods, baseline CP yields high profit, but can be infeasible and requires much more training and test time. Except for PPO, UVP/CP and WS/PC/CP offer the best trade-off between profit, training, and test time, while UVP and WS/PC achieve lower profits with lower test time. Each AM-P generalizes well: SAC and PPO improve average profit by 3% and 2% on unseen test instances. Thus, our AM-P uniquely outperforms the state-of-the-art, demonstrating a general approach for stochastic, dynamic sequential problems with state-dependent constraints.

**Ablation Study.** Table 2 also presents an ablation study. Removing FR from FR/UVP increases profit significantly for SAC and slightly for PPO without affecting feasibility. Similarly, removing FR from FR/WS/PC increases profit and maintains feasibility for both DRL methods. Though surprising without stability mechanisms, the performance aligns with the principle that vessels stabilize with higher utilization. Replacing SAC with PPO for action-gradient flow increases profit but also violations in FR and PD (see Appendix ), while projection mitigates this effect.

## Managerial Insights

Figure 5 performs sensitivity analyses on SMIP scenario size, demand uncertainty, and voyage length, reporting averages and 95% confidence intervals with  $N = 30$ . We use the same hyperparameters as Table 2 unless stated otherwise.

**Value of Information.** Figure 5a compares profits under non-anticipation, imperfect, and perfect information. As scenario sizes grow, the SMIP predictive accuracy improves and profits stabilize. At 28 scenarios, perfect information increases profits by 60–65% over non-anticipation, while DRL with imperfect information improves profits by 30–40%, showing the impact of information on decision quality.

**Computational Time.** While inference time is crucial, training time also matters. Figure 5b shows computational time for 30 instances. SMIP-NA’s time grows exponentially with scenarios, reaching 2 hours per instance at 28 scenarios, while SMIP-PI grows steadily. SAC trains offline in 1–3

Methods			Train	Testing ( $N = 30$ )			Generalization ( $N = 30$ )		
Alg.	Model	F.M.	Time (s)	Obj. (\$)	Time (s)	Feas. (%)	Obj. (\$)	Time (s)	Feas. (%)
SAC	AM-P	UVP	11,781	1,451.30	0.74	100.00	1,476.74	0.74	100.00
SAC	AM-P	FR/UVP	7,612	1,327.03	0.65	100.00	1,413.26	0.69	100.00
SAC	AM-P	UVP/CP	11,781	1,479.41	1.32	100.00	1,505.32	1.33	100.00
SAC	AM-P	WS/PC	9,015	1,474.17	0.67	100.00	1,500.57	0.67	100.00
SAC	AM-P	FR/WS/PC	7,201	1,370.14	0.68	100.00	1,399.58	0.68	100.00
SAC	AM-P	WS/PC/CP	9,015	1,479.02	1.32	100.00	1,504.69	1.32	100.00
SAC	AM	FR	2,443	1,188.90	0.76	0.00	1,196.70	1.12	0.00
SAC	AM	PD	5,205	1,077.84	0.76	0.00	1,085.58	0.87	0.00
SAC	AM-P	CP	85,031	1,482.56	11.74	100.00	1,509.05	11.80	100.00
PPO	AM-P	UVP	15,517	1,353.58	0.97	100.00	1,373.96	0.97	100.00
PPO	AM-P	FR/UVP	16,585	1,328.10	0.67	100.00	1,350.19	0.67	100.00
PPO	AM-P	UVP/CP	15,517	1,482.72	1.33	100.00	1,508.85	1.33	100.00
PPO	AM-P	WS/PC	21,860	1,453.53	0.67	100.00	1,471.66	0.67	100.00
PPO	AM-P	FR/WS/PC	4,885	1,331.02	0.67	100.00	1,353.19	0.67	100.00
PPO	AM-P	WS/PC/CP	21,860	1,480.45	4.70	86.67	1,508.78	4.65	93.33
PPO	AM	FR	5,800	1,294.31	0.75	0.00	1306.85	1.43	0.00
PPO	AM	PD	7,331	1,149.44	1.42	0.00	1,152.83	0.75	0.00
PPO	AM-P	CP	233,959	1,479.25	11.21	96.67	1,499.46	8.28	100.00
CPL	SMIP-NA	-	-	1,053.02	8,434.58	100.00	1,023.04	8,434.94	100.00
CPL	SMIP-PI*	-	-	1,713.73	40.75	100.00	1,680.51	38.93	100.00

Table 2: AM-P versus baselines with various algorithms (Alg.) and feasibility mechanisms (F.M.).

hours, and PPO takes 1–12 hours, except for AM-P with CP, which requires significantly longer. Inference is near-instant for all. Amortized, SAC and PPO average 8 and 10 minutes per instance, making DRL more efficient than SMIP-NA.

**Adaptiveness.** Figure 5c shows how policies adapt to demand uncertainty by varying the coefficient of variation across unseen instances. As variability and uncertainty increase, both SAC and PPO policies achieve higher average profits by exploiting demand outliers, demonstrating their ability to leverage uncertainty. Despite fluctuations in variability, both policies consistently generate feasible solutions.

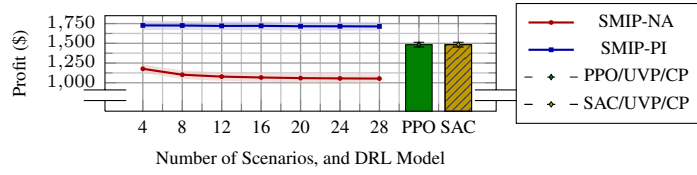
**Scalability.** Figure 5d shows policies trained on  $|P| = 4$  achieve 80–90% of maximum revenue when deployed on voyages with  $|P| \in 5, 6$ , demonstrating effective generalization to longer voyages. Inference costs scale linearly with problem sizes, while each solution remains feasible. Note that scaling to larger vessels currently requires retraining.

**Deployment Challenges.** Due to limited data availability, we simulate instances matching demand to capacity, as in industry. For industrial deployment, generating representative data and extending differentiable projection to non-convex constraints are key. Finally, integrating MPP with SPP, uptake, and cargo flow management is possible, but it adds significant complexity and decision interdependencies.

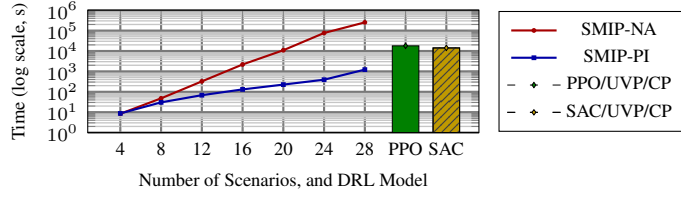
## Conclusion and Future Directions

We introduce a stochastic dynamic MDP with state-dependent constraints for MPP under demand uncertainty,

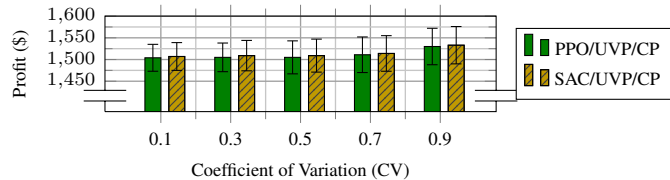
addressing a class of challenges often overlooked. We propose a general AM policy with unbiased feasibility projections, trained via actor-critic DRL. Our policy uniquely surpasses state-of-the-art baselines by efficiently generating feasible, high-profit solutions that scale and adapt to diverse instances of a complex problem. Although demonstrated on the MPP, our architecture is a general approach for constrained sequential decision-making under uncertainty. It highlights the importance of AI decision support in practical planning, impacting supply chain reliability and sustainability. Future work on non-convex projections, scalability, and new planning problems will tackle real-world AI challenges.



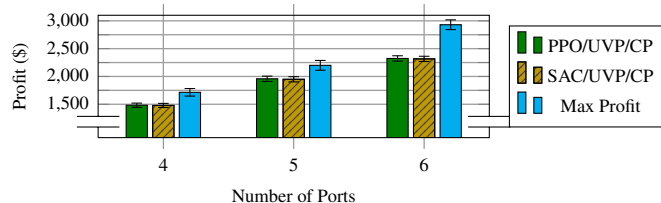
(a) Profit across scenario sizes on test instances.



(b) Computational time across scenario sizes on test instances.



(c) Profit across CV levels on generalization instances.



(d) Profit across voyage lengths on generalization instances.

Figure 5: Sensitivity analyses.

## Ethical Statement

Human oversight is critical in container shipping decision-support tools for fairness, accountability, and transparency. While models enhance decision-making and provide optimized, feasible plans, human judgment remains essential, especially in safety-critical situations like vessel stability and dangerous cargo. Optimizing solely for revenue might inadvertently bias cargo prioritization, impacting customers and voyages. Safeguards are encouraged to mitigate automation bias, allowing users to challenge outputs and ensuring continuous validation and auditing for trust and fairness in cargo placement. Efficient vessel utilization also contributes to reducing fuel consumption and greenhouse gas emissions.

## References

Agrawal, A.; Amos, B.; Barratt, S.; and Boyd, S. 2019. Differentiable Convex Optimization Layers. In *Advances in Neural Information Processing Systems*.

Alshiekh, M.; Bloem, R.; Ehlers, R.; Könighofer, B.; Niekum, S.; and Topcu, U. 2018. Safe Reinforcement Learning via Shielding. In *Proceedings of the AAAI Conference on Artificial Intelligence*, volume 32.

Bengio, Y.; Lodi, A.; and Prouvost, A. 2021. Machine learning for combinatorial optimization: A methodological tour d'horizon. *European Journal of Operational Research*, 290(2): 405–421.

Biewald, L. 2020. Experiment Tracking with Weights and Biases. Software available from wandb.com.

Bilican, M. S.; Evren, R.; and Karatas, M. 2020. A Mathematical Model and Two-Stage Heuristic for the Container Stowage Planning Problem with Stability Parameters. *IEEE Access*, 8: 113392–113413.

Birge, J.; and Louveaux, F. 2011. *Introduction to Stochastic Programming*. Springer Series in Operations Research and Financial Engineering. Springer New York. ISBN 978-1-4614-0237-4.

Bishop, C. M. 2006. *Pattern recognition and machine learning*. Information science and statistics. New York: Springer. ISBN 978-0-387-31073-2.

Boland, N.; Christiansen, J.; Dandurand, B.; Eberhard, A.; Linderoth, J.; Luedtke, J.; and Oliveira, F. 2018. Combining Progressive Hedging with a Frank-Wolfe Method to Compute Lagrangian Dual Bounds in Stochastic Mixed-Integer Programming. *SIAM Journal on Optimization*, 28(2): 1312–1336.

Boyd, S. P.; and Vandenberghe, L. 2004. *Convex optimization*. Cambridge New York Melbourne New Delhi Singapore: Cambridge University Press, version 29 edition. ISBN 978-0-521-83378-3.

Calvo-Fullana, M.; Paternain, S.; Chamon, L. F. O.; and Ribeiro, A. 2021. State Augmented Constrained Reinforcement Learning: Overcoming the Limitations of Learning With Rewards. *IEEE Transactions on Automatic Control*, 69: 4275–4290.

Chang, Y.; Hamed, M.; and Haghani, A. 2022. Solving integrated problem of stowage planning with crane split by an improved genetic algorithm based on novel encoding mode. *Measurement and Control*.

Chen, R.; and Luedtke, J. 2022. On sample average approximation for two-stage stochastic programs without relatively complete recourse. *Mathematical Programming*, 196(1-2): 719–754.

Chen, W.; Tanneau, M.; and Van Hentenryck, P. 2024. End-to-End Feasible Optimization Proxies for Large-Scale Economic Dispatch. *IEEE Transactions on Power Systems*, 39(2): 4723–4734.

Ding, D.; Zhang, K.; Basar, T.; and Jovanovic, M. 2020. Natural Policy Gradient Primal-Dual Method for Constrained Markov Decision Processes. In Larochelle, H.; Ranzato, M.; Hadsell, R.; Balcan, M. F.; and Lin, H., eds., *Advances in Neural Information Processing Systems*, volume 33, 8378–8390. Curran Associates, Inc.

Donti, P. L.; Rolnick, D.; and Kolter, J. Z. 2021. DC3: A learning method for optimization with hard constraints. In *Proceedings of the 9th International Conference on Learning Representations*.

European Commission. 2023. Reducing Emissions from the Shipping Sector.

Fujita, Y.; and Maeda, S.-i. 2018. Clipped Action Policy Gradient. In *Proceedings of the 35th International Conference on Machine Learning*.

Haarnoja, T.; Zhou, A.; Abbeel, P.; and Levine, S. 2018. Soft Actor-Critic: Off-Policy Maximum Entropy Deep Reinforcement Learning with a Stochastic Actor. In *Proceedings of the 35th International Conference on Machine Learning*. PMLR.

Herup, M. O.; Thiesgaard, G. C. W.; Van Twiller, J.; and Jensen, R. M. 2022. A Linear Time Algorithm for Optimal Quay Crane Scheduling. In *Computational Logistics*, volume 13557, 60–73. Barcelona, Spain: Springer Nature Switzerland.

Hottung, A.; Kwon, Y.-D.; and Tierney, K. 2022. Efficient Active Search for Combinatorial Optimization Problems. In *Proceedings of the International Conference on Learning Representations*.

Hottung, A.; Tanaka, S.; and Tierney, K. 2020. Deep learning assisted heuristic tree search for the container pre-marshalling problem. *Computers & Operations Research*, 113: 104781.

Jensen, R. M.; Pacino, D.; Ajspur, M. L.; and Vesterdal, C. 2018. *Container Vessel Stowage Planning*. Weilbach. ISBN 978-87-7790-311-3.

Kanervisto, A.; Scheller, C.; and Hautamäki, V. 2020. Action Space Shaping in Deep Reinforcement Learning. In *2020 IEEE Conference on Games (CoG)*.

Kool, W.; van Hoof, H.; and Welling, M. 2019. Attention, Learn to Solve Routing Problems! In *Proceedings of the International Conference on Learning Representations*.

Kwon, Y.-D.; Choo, J.; Kim, B.; Yoon, I.; Gwon, Y.; and Min, S. 2020. POMO: Policy Optimization with Multiple Optima for Reinforcement Learning. In *Proceedings of the 34th Conference on Neural Information Processing Systems*.

Lloyd's List. 2022. Shipping emissions rise 4.9% in 2021.

Martin-Iradi, B.; Pacino, D.; and Ropke, S. 2022. The Multiport Berth Allocation Problem with Speed Optimization: Exact Methods and a Cooperative Game Analysis. *Transportation Science*, 56(4): 972–999.

Pacino, D. 2018. Crane Intensity and Block Stowage Strategies in Stowage Planning. In *Computational Logistics*, volume 11184 LNCS, 191–206. Springer.

Pacino, D.; Delgado, A.; Jensen, R.; and Bebbington, T. 2011. Fast generation of near-optimal plans for eco-efficient stowage of large container vessels. *Computational Logistics*, 286–301.

Parreño-Torres, C.; Çalık, H.; Alvarez-Valdes, R.; and Ruiz, R. 2021. Solving the generalized multi-port container stowage planning problem by a matheuristic algorithm. *Computers and Operations Research*, 133: 105383–105383. Publisher: Elsevier Ltd.

Powell, W. B. 2022. *Reinforcement Learning and Stochastic Optimization: A Unified Framework for Sequential Decisions*, volume 22. Wiley, 1st edition. ISBN 978-1-119-81505-1.

Rahmaniani, R.; Crainic, T. G.; Gendreau, M.; and Rei, W. 2017. The Benders decomposition algorithm: A literature review. *European Journal of Operational Research*, 259(3): 801–817.

Roberti, R.; and Pacino, D. 2018. A decomposition method for finding optimal container stowage plans. *Transportation Science*, 52(6): 1444–1462.

Römisch, W. 2009. Scenario Reduction Techniques in Stochastic Programming. In Watanabe, O.; and Zeugmann, T., eds., *Stochastic Algorithms: Foundations and Applications*, volume 5792, 1–14. Berlin, Heidelberg: Springer Berlin Heidelberg. ISBN 978-3-642-04943-9 978-3-642-04944-6. Series Title: Lecture Notes in Computer Science.

Schulman, J.; Moritz, P.; Levine, S.; Jordan, M. I.; and Abbeel, P. 2016. High-Dimensional Continuous Control Using Generalized Advantage Estimation. In *4th International Conference on Learning Representations*.

Schulman, J.; Wolski, F.; Dhariwal, P.; Radford, A.; and Klimov, O. 2017. Proximal Policy Optimization Algorithms. ArXiv:1707.06347.

Shapiro, A. 2011. Analysis of stochastic dual dynamic programming method. *European Journal of Operational Research*, 209(1): 63–72.

Tierney, K.; Pacino, D.; and Jensen, R. M. 2014. On the complexity of container stowage planning problems. *Discrete Applied Mathematics*, 169: 225–230.

United Nations Conference on Trade and Development. 2021. Review of Maritime Transport 2021. Technical report, United Nations.

Van Twiller, J.; Sivertsen, A.; Jensen, R. M.; and Andersen, K. H. 2024a. An Efficient Integer Programming Model for Solving the Master Planning Problem of Container Vessel Stowage. In *Computational Logistics*, 236–253. Monterrey, Mexico: Springer Nature Switzerland.

Van Twiller, J.; Sivertsen, A.; Pacino, D.; and Jensen, R. M. 2024b. Literature survey on the container stowage planning problem. *European Journal of Operational Research*, 317(3): 841–857.

Vaswani, A.; Shazeer, N.; Parmar, N.; Uszkoreit, J.; Jones, L.; Gomez, A. N.; Kaiser, L.; and Polosukhin, I. 2017. Attention is All you Need. In *Advances in Neural Information Processing Systems*, volume 30. Curran Associates, Inc.

Vinyals, O.; Fortunato, M.; and Jaitly, N. 2015. Pointer Networks. In Cortes, C.; Lawrence, N.; Lee, D.; Sugiyama, M.; and Garnett, R., eds., *Advances in Neural Information Processing Systems*, volume 28. Curran Associates, Inc.

Wang, Y.; Zhan, S. S.; Jiao, R.; Wang, Z.; Jin, W.; Yang, Z.; Wang, Z.; Huang, C.; and Zhu, Q. 2023. Enforcing Hard Constraints with Soft Barriers: Safe Reinforcement Learning in Unknown Stochastic Environments. In *Proceedings of the 40th International Conference on Machine Learning*.

Zhang, L.; Shen, L.; Yang, L.; Chen, S.; Wang, X.; Yuan, B.; and Tao, D. 2022. Penalized Proximal Policy Optimization for Safe Reinforcement Learning. In *Proceedings of the Thirty-First International Joint Conference on Artificial Intelligence*, 3744–3750. Vienna, Austria: International Joint Conferences on Artificial Intelligence Organization.

## MDP of Master Planning Problem

### Sets and Parameters

Provided the sets and parameters in Section , we introduce additional subsets of the transport set  $TR$  given port  $p \in P$ :

- Onboard transports:  $TR_p^{OB} = \{(i, j) \in P^2 \mid i \leq p, j > p\}$
- Arrival transports:  $TR_p^{ROB} = \{(i, j) \in P^2 \mid i < p, j > p\}$
- Load transports:  $TR_p^+ = \{(p, j) \in P^2 \mid j > p\}$
- Discharge transports:  $TR_p^- = \{(i, p) \in P^2 \mid i < p\}$
- Transports in crane operations:  $TR_p^M = TR_p^+ \cup TR_p^-$

Considering episode parameters  $\zeta$ , we define:

- Transports:  $tr = (i, j) \in TR$
- Cargo types:  $k = (\kappa_1, \kappa_2, \kappa_3) \in K$

For each combination  $(i, j, k)$ , we associate the expected demand  $\mu^{(i, j, k)}$ , standard deviation  $\sigma^{(i, j, k)}$ , TEU per container  $teu^{(i, j, k)}$ , container weight  $w^{(i, j, k)}$ , and revenue per container  $rev^{(i, j, k)}$ . These are all combined in the instance parameter  $\zeta^{(i, j, k)} \forall (i, j) \in TR, k \in K$

The TEU per container depends on  $k$  as:

$$teu(k) = \begin{cases} 1, & \text{if } \kappa_1 = 20 \text{ ft.} \\ 2, & \text{if } \kappa_1 = 40 \text{ ft.} \end{cases} .$$

Similarly, the container weight is defined by:

$$w(k) = \begin{cases} 1, & \text{if } \kappa_2 = \text{Light} \\ 2, & \text{if } \kappa_2 = \text{Medium} \\ 3, & \text{if } \kappa_2 = \text{Heavy} \end{cases} .$$

Both  $teu$  and  $w$  are broadcasted to shape  $n_q = |K| \times |TR|$  in the MDP formulations for consistency in dimensionality.

The revenue function is given by:

$$rev(i, j, k) = \begin{cases} (j - i)(1 - LR) + 0.1, & \text{if } \kappa_3 = \text{Long} \\ (j - i) + 0.1, & \text{if } \kappa_3 = \text{Spot} \end{cases} .$$

The expected value  $\mu \in \mathbb{R}_{\geq 0}^{n_q}$  and standard deviation  $\sigma \in \mathbb{R}_{>0}^{n_q}$  of demand are randomly generated, as will be described in Appendix .

### MDP

We define the MDP by decomposing the traditional CO problem outlined in Van Twiller et al. (2024a).

In the traditional MPP, cargo is loaded onto a vessel at each port in a voyage. Let  $u \in \mathbb{R}^{n_u}$  represent the vessel's utilization over the voyage, which is defined by the set of ports  $P = \{1, 2, \dots, N_P\}$ . Let us also recall the following:

$$n_u = |B| \times |D| \times |K| \times |TR|$$

$$n_c = |B| \times |D|, \quad n_q = |K| \times |TR| \quad n_u = \{n_c \times n_q\}$$

Utilization  $u$  can be decomposed into individual voyage legs, corresponding to the segments between consecutive ports. Specifically, we decompose as:

$$u = (u_0, u_1, \dots, u_{N_P-1})$$

where each  $u_p \in \mathbb{R}^{n_u}$  represents the vessel's utilization immediately after operations at port  $p$ .

**Feasible Region** Suppose we have a feasible region for the MPP, where:

- $A' \in \mathbb{R}^{m_u \times n_u}$  is the constraint matrix,
- $b' \in \mathbb{R}^{m_u}$  is the bound vector,
- $u_p \in \mathbb{R}_{\geq 0}^{n_u}$  is the nonnegative vessel utilization.

The feasible region, denoted as  $PH$ , is given by:

$$PH(s_p) = \{u_p \in \mathbb{R}_{\geq 0}^{n_u} \mid A' u_p \leq b'\} .$$

At port  $p$ , utilization can be decomposed into load operations and pre-load utilization:

$$u_p = u'_p + u_p^+,$$

where:

- $u_p^+ \in \mathbb{R}_{\geq 0}^{n_u}$  represents load operations,
- $u'_p = u_{p-1} - u_p^-$  is the utilization before load operations,
- $u_{p-1} \in \mathbb{R}_{\geq 0}^{n_u}$  is the previous step's utilization,
- $u_p^- \in \mathbb{R}_{\geq 0}^{n_u}$  is the discharge operations.

Consequently, we can rewrite the feasible region as:

$$PH(s_p) = \{u_p^+ \in \mathbb{R}_{\geq 0}^{n_u} \mid A' u_p^+ \leq b' - A' u'_p\} .$$

### Decomposed MDP

Utilization can be decomposed into sequential steps to refine temporal granularity, thereby obtaining an decomposed MDP formulation. We decompose  $u$  as:

$$u = (u_0, u_1, \dots, u_{T_{seq}}) ,$$

where  $u_t \in \mathbb{R}^{n_u}$  represents the utilization at time step  $t$ , and  $t \in H = \{1, 2, \dots, T_{seq}\}$  denotes the episodic horizon  $H$ .

Each step  $t$  represents a transport and cargo type, as tuple  $(pol_t, pod_t, k_t)$ . Algorithm 2 illustrates an episode of the decomposed MDP. First, we reset the state  $s_0$ , initialize time  $t$ , and an empty trajectory. The episode iterates over load ports ( $pol_t$ ), discharge ports ( $pod_t$ ), and cargo classes ( $k_t$ ). At each step, we sample action  $x_t$  from policy  $\pi_\theta(x|s_t)$  conditioned on state  $s_t$  and episode parameters  $\zeta$ , and transition to state  $s_{t+1}$ . Afterwards, we store the results in the trajectory and increment time  $t$ . This process continues until all combinations of  $pol_t$ ,  $pod_t$ , and  $k_t$  are explored, accumulating a total of  $T_{seq}$  steps.

**Transitions** We use a stochastic transition function  $\mathcal{T}(s_{t+1}|s_t, x_t, \zeta) \in \Delta(S)$ . The transition consists of sequential steps:

1. If  $t \in T_{\text{new port}}$ , port demand is revealed. This means we show  $q_t^{(i, j, k)} \forall (i, j) \in TR_{pol_t}^+, k \in K$ .
2. If  $t \in T_{\text{new port}}$ , onboard cargo is discharged  $u_{t+1} = u_t \odot (1 - \mathbf{e}_t^-)$ , where  $\mathbf{e}_t^- \in \{0, 1\}^{n_q}$  is a binary mask indicating the cargo type and transport to nullify in  $u_t$ .
3. Each time  $t$ , cargo is loaded onboard  $u_{t+1} = u_t + x_t \odot \mathbf{e}_t^+$ , where  $\mathbf{e}_t^+ \in \{0, 1\}^{n_q}$  is a binary indicator specifying cargo types and transports to add to  $u_t$ .

---

**Algorithm 2: Episode of Decomposed MDP**


---

**Require:**  $\mathcal{T}, \pi_\theta, \zeta, \mathcal{Q}$

- 1:  $q_{T_{\text{seq}}}^{(i,j,k)} \sim \mathcal{Q}(\mu^{(i,j,k)}, \sigma^{(i,j,k)}) \forall (i,j) \in TR, k \in K$
- 2:  $s_0 \leftarrow (\mathbf{0}^{n_u}, q_{T_{\text{seq}}} \odot \mathbf{e}_0^+), t \leftarrow 0, \text{Trajectory} \leftarrow \{\}$
- 3: **for**  $pol_t = 1$  to  $N_P - 1$  **do**
- 4:   **for**  $pod_t = pol_t + 1$  to  $N_P$  **do**
- 5:     **for**  $k_t \in K$  **do**
- 6:        $x_t \sim \pi_\theta(x|s_t, \zeta)$
- 7:        $s_{t+1} \sim \mathcal{T}(s_t, x_t, \zeta)$
- 8:       Append  $(s_t, x_t, r_t, s_{t+1})$  to Trajectory
- 9:        $t \leftarrow t + 1$
- 10:   **end for**
- 11:   **end for**
- 12: **end for**
- 13: **return** Trajectory

---

Additionally, we define the set of time steps before we leave for a new port  $p + 1$  is defined as follows:

$$T_{\text{leave port}} = \left\{ t \in H \mid \exists p \in P_1^{N_P-1} \text{ such that } t = |K| \left( p(N_P - 1) - \frac{p(p-1)}{2} \right) - 1 \right\}.$$

Finally, the set of time steps at which we arrive at a new port  $p$  is defined as follows:

$$T_{\text{new port}} = \left\{ t \in H \mid \exists p \in P_1^{N_P-1} \text{ such that } t = |K| \left( (p-1)(N_P - 1) - \frac{p(p-1)}{2} \right) \right\}.$$

**Feasible Region** The state-dependent feasible region for each time  $t$  is formulated as:

$$PH(s_t) = \{u_t \in \mathbb{R}_{\geq 0}^{n_u} \mid A' u_t \leq b'\}$$

Similar to the port utilization, utilization can be decomposed into load operations and pre-load utilization:

$$u_t = u'_t + u_t^+$$

where:

- $u_t^+ \in \mathbb{R}_{\geq 0}^{n_u}$  represents load operations,
- $u'_t = u_{t-1} - u_t^-$  is the utilization before load operations,
- $u_{t-1} \in \mathbb{R}_{\geq 0}^{n_u}$  is the previous step's utilization,
- $u_t^- \in \mathbb{R}_{\geq 0}^{n_u}$  is the discharge operations.

Using the decomposition, we obtain the feasible region as:

$$PH(s_t) = \{u_t \in \mathbb{R}_{\geq 0}^{n_u} \mid A'(u_t^+ + u'_t) \leq b'\}$$

**Substituting Load Operations for Actions** Actions  $x_t$  correspond to transformed load operations  $u_t^+$ , given by:

$$x_t = u_t^+ M(s_t), \quad M(s_t) \in \{0, 1\}^{n_u \times n_c},$$

where  $M(s_t)$  is a state-dependent sparsity mask that selects relevant elements from  $u_t^+$ .

However, load operations are subject to  $m_u$  constraints, whereas actions adhere to  $m_c$  constraints. To bridge this difference, we define the state-dependent constraint matrix:

$$A(s_t) = T(s_t)^\top A' M(s_t), \quad T(s_t) \in \{0, 1\}^{m_u \times m_c},$$

where:

- $A'$  is the original constraint matrix of shape  $(m_u, n_u)$ ,
- $T(s_t)$  maps the constraints of  $u_t^+$  to that of  $x_t$
- $M(s_t)$  maps the space of  $u_t^+$  to that of  $x_t$ ,

Similarly, we introduce a state-dependent bound:

$$b''(s_t) = T(s_t)^\top b',$$

where:

- $b'$  is the original bound of shape  $(m_u, 1)$ ,
- $T(s_t)$  maps the constraints of  $u_t^+$  to that of  $x_t$

**Feasible Region for Actions** Using the refined notation, we express the state-dependent feasible region in terms of actions:

$$PH(s_t) = \{x_t \in \mathbb{R}_{\geq 0}^{n_c} \mid A(s_t)x_t \leq b''(s_t) - A' u'_t\}.$$

Next, we define the updated bound as:

$$b(s_t) = b''(s_t) - A' u'_t.$$

Substituting this into the feasible region, we obtain:

$$PH(s_t) = \{x_t \in \mathbb{R}_{\geq 0}^{n_c} \mid A(s_t)x_t \leq b(s_t)\}.$$

### MPP Constraints

Let us specify the MPP constraints of  $PH(s_p)$  and  $PH(s_t)$ .

**Demand Constraints** Let us consider the demand subset of  $PH(s_p)$  as:

$$PH(s_p)_{\text{dem}} = \{x_p \in \mathbb{R}_{\geq 0}^{n_u} \mid A'_{\text{dem}} x_p \leq b'_{\text{dem}} - A'_{\text{dem}} u'_p\}.$$

We sum over all vessel locations to obtain an aggregated number of containers of shape  $n_q$ . Note that only current load actions  $x_p$  are relevant for  $q_p$ , hence we can omit  $A'_{\text{dem}} u'_p$  as pre-loading utilization has already satisfied its demand requirements.

$$x_p^\top \mathbf{1}_{n_c} \leq q_p$$

Consider the demand subset of  $PH(s_t)$  as:

$$PH(s_t)_{\text{dem}} = \{x_t \in \mathbb{R}_{\geq 0}^{n_c} \mid A(s_t)_{\text{dem}} x_t \leq b'(s_t)_{\text{dem}} - A'_{\text{dem}} u'_t\}.$$

Right now, we can sum the full vector  $x_t$  as it needs to sum to scalar  $q_t^{(pol_t, pod_t, k_t)}$ . Again, previous steps are irrelevant to demand, hence we can disregard  $A'_{\text{dem}} u'_t$  to obtain:

$$\mathbf{1}^\top x_t \leq q_t^{(pol_t, pod_t, k_t)}$$

**Capacity Constraints** Let us consider the constraint subset of  $PH(s_p)$  as:

$$PH(s_p)_{\text{cap}} = \{x_p \in \mathbb{R}_{\geq 0}^{n_u} \mid A'_{\text{cap}} x_p \leq b'_{\text{cap}} - A'_{\text{cap}} u'_p\}.$$

We sum TEU of all cargo types and transports in  $x_p$  to obtain TEU use per location with shape  $n_c$ . The TEU of pre-load utilization is also considered by subtracting it from the vessel capacity, obtaining the following:

$$x_p \text{teu} \leq c - u'_p \text{teu},$$

Consider the demand subset of  $PH(s_t)$  as:

$$PH(s_t)_{\text{cap}} = \{x_t \in \mathbb{R}_{\geq 0}^{n_c} \mid A(s_t)_{\text{cap}} x_t \leq b'(s_t)_{\text{cap}} - A'_{\text{cap}} u'_t\}.$$

Now, we can do the same trick based on a single scalar  $\text{teu}^{(pol_t, pod_t, k_t)}$  multiplied with the sum of action  $x_t$ .

$$\text{teu}^{(pol_t, pod_t, k_t)} \mathbf{1}^\top x_t \leq c - u'_t \text{teu},$$

**Stability Constraints** The stability constraints require some algebra to derive for  $PH(s_p)$  and  $PH(s_t)$ .

The lcg constraint in its original form is given by:

$$\frac{\mathbf{1}^\top (lm \odot u_p)}{\mathbf{1}^\top (w \odot u_p)} \leq \overline{lcg}.$$

Applying the utilization decomposition, we can obtain the formulation for  $PH(s_p)$ :

$$\begin{aligned} \mathbf{1}^\top (lm \odot u_p) &\leq \overline{lcg} \mathbf{1}^\top (w \odot u_p) \\ \mathbf{1}^\top (lm \odot u_p^+) + \mathbf{1}^\top (lm \odot u_p') &\leq \overline{lcg} \mathbf{1}^\top (w \odot u_p^+) \\ &\quad + \overline{lcg} \mathbf{1}^\top (w \odot u_p') \\ \mathbf{1}^\top (lm_p \odot x_p) - \overline{lcg} \mathbf{1}^\top (w \odot x_p) &\leq \overline{lcg} \mathbf{1}^\top (w \odot u_p') \\ &\quad - \mathbf{1}^\top (lm \odot u_p') \\ \mathbf{1}^\top ((lm - \overline{lcg}w) \odot x_p) &\leq \mathbf{1}^\top ((\overline{lcg}w - lm) \odot u_p'). \end{aligned}$$

This approach extends to both the lower and upper bounds for the lcg and vcg, ensuring that vessel stability is properly maintained at every step.

Based on the  $PH(s_p)$  constraint, we can substitute load operations for actions, and obtain the formulation for  $PH(s_t)$ :

$$\mathbf{1}^\top ((lm(t) - \overline{lcg}w(t)) \odot x_t) \leq \mathbf{1}^\top ((\overline{lcg}w - lm) \odot u'_p).$$

where  $w(t) = w^{(pol_t, pod_t, k_t)}$  and  $lm(t) = lm^{(pol_t, pod_t, k_t)}$

## Auxiliary Variables

The reward function contains two auxiliary variables derived from state  $s$ , which incur costs due to inefficient port operations. At port  $p$ , Equation (14) creates an indicator of hatch movements  $hm(s, p) \in \{0, 1\}^{|B|}$ , whereas Equation (15) computes the number of on-deck containers during hatch movements, causing hatch overstayage  $ho(s, p) \in \mathbb{R}_{\geq 0}^{|B|}$ .

$$hm(s, p) = \left( \sum_{k \in K} \sum_{tr \in TR_p^M} u_t^{(b, d^{\text{above}}, k, tr)} > 0 \right) \quad (14)$$

$$ho(s, p) = hm(s, p) \left( \sum_{k \in K} \sum_{tr \in TR_p^{\text{ROB}}} u_t^{(b, d^{\text{above}}, k, tr)} \right) \quad (15)$$

Equation (16) computes the target crane moves at port  $p$  by equally spreading the total demand per port over pairs of adjacent bays, where  $\delta^{cm}$  is the allowed deviation from the equal spread set by ports. Subsequently, Equation (17) computes the excess crane moves  $cm(s, p) \in \mathbb{R}_{\geq 0}^{|B|-1}$

$$\overline{cm}(s, p) = (1 + \delta^{cm}) \frac{2}{|B|} \sum_{tr \in TR_p^M} \sum_{k \in K} q_t^{(tr, k)} \quad (16)$$

$$\begin{aligned} cm(s, p) = \max \left( \sum_{d \in D} \sum_{k \in K} \sum_{tr \in TR_p^M} u_t^{(0:|B|-1, d, k, tr)} \right. \\ \left. + u_t^{(1:|B|, d, k, tr)} - \overline{cm}(s, p), 0 \right) \quad (17) \end{aligned}$$

## Feasibility Mechanisms

### Log Probability Adjustments

This subsection provides technical details on the adjustments to the log-probability distribution of the policy as a result of non-linear transformations to distribution samples.

Projecting actions alters the policy's probability density, necessitating consideration of the change of variables principle (Bishop 2006). This principle ensures valid volume scaling by requiring the transformation  $f(x)$  to satisfy:

- Differentiability:**  $f(x)$  must be differentiable to compute the Jacobian  $J_f(x)$  and determine local volume scaling.
- Non-Singularity:** The Jacobian determinant must be non-zero ( $\det(J_f(x)) \neq 0$ ) to prevent dimensional collapse.
- Invertibility:**  $f(x)$  must be locally or globally invertible to ensure a one-to-one mapping between points in the original and transformed spaces.

These properties ensure the transformation is smooth, one-to-one, and well-behaved, enabling the use of the Jacobian adjustment  $\log \pi'(x|s) = \log \pi(x|s) - \log |\det(J_f(x))|$  as a valid probability scaling factor.

**Weighted Scaling Projection Layer** Suppose we have variable  $x \in \mathbb{R}_{>0}^n$  and scalar  $y \in \mathbb{R}_{>0}$  and the following piecewise linear function:

$$\mathcal{P}(x, y) = \begin{cases} x & \text{if } \mathbf{1}^\top x \leq y \\ \frac{x}{\mathbf{1}^\top x} \cdot y & \text{if } \mathbf{1}^\top x > y \end{cases}$$

Case 1:  $\mathbf{1}^\top x \leq y$ .

$$\begin{aligned} \mathcal{P}(x, y) &= x \\ \frac{\partial}{\partial x} \mathcal{P}(x, y) &= \frac{\partial x}{\partial x} \\ J_{\mathcal{P}}(x, y) &= I_n \end{aligned}$$

Case 2:  $\mathbf{1}^\top x > y$ , where we apply the product rule and then the quotient rule of differentiation.

$$\begin{aligned}\mathcal{P}(x, y) &= \frac{x}{\mathbf{1}^\top x} \cdot y \\ \frac{\partial}{\partial x} \mathcal{P}(x, y) &= \frac{\partial}{\partial x} \left( \frac{x}{\mathbf{1}^\top x} \cdot y \right) \\ \frac{\partial}{\partial x} \mathcal{P}(x, y) &= \frac{\partial}{\partial x} \left( \frac{x}{\mathbf{1}^\top x} \right) \cdot y \\ J_{\mathcal{P}}(x, y) &= y \cdot \frac{1}{(\mathbf{1}^\top x)^2} (I_n \mathbf{1}^\top x - x \cdot \mathbf{1}^\top) \\ J_{\mathcal{P}}(x, y) &= \frac{y \cdot I_n}{(\mathbf{1}^\top x)} - \frac{y \cdot x^\top}{(\mathbf{1}^\top x)^2}\end{aligned}$$

We obtain the following Jacobian of function  $\mathcal{P}(x, y)$ :

$$J_{\mathcal{P}}(x, y) = \begin{cases} I_n & \text{if } \mathbf{1}^\top x \leq y \\ \frac{y}{(\mathbf{1}^\top x)^2} (I_n \mathbf{1}^\top x - x \mathbf{1}^\top) & \text{if } \mathbf{1}^\top x > y \end{cases}$$

Finally, we verify that Jacobian adjustment is allowed for the weighted scaling projection by:

1.  $\mathcal{P}(x, y)$  has been shown to be differentiable.
2. Provided that  $x, y > 0$ , either case is positive definite as the diagonal elements are strictly positive. We obtain  $\det(J_{\mathcal{P}}(x, y)) > 0$ , thus the Jacobian is non-singular.
3.  $\mathcal{P}(x, y)$  is locally invertible as  $\det(J_{\mathcal{P}}(x, y)) \neq 0$ .

**Unbiased Violation Projection** Suppose we have function  $\mathcal{P}(x, A, b) = x - \eta_v A^\top (Ax - b)_{>0}$  with  $x \in \mathbb{R}_{>0}^n$ ,  $\eta_v \in \mathbb{R}_{>0}$ ,  $A \in \mathbb{R}_{\geq 0}^{m \times n}$ ,  $b \in \mathbb{R}_{\geq 0}^m$ , and  $m > n$ .

Case 1:  $\eta_v A^\top (Ax - b) = 0$ .

$$\begin{aligned}\mathcal{P}(x, A, b) &= x \\ \frac{\partial}{\partial x} \mathcal{P}(x, A, b) &= \frac{\partial x}{\partial x} \\ J_{\mathcal{P}}(x, A, b) &= I_n\end{aligned}$$

Case 2:  $\eta_v A^\top (Ax - b) > 0$ , where we apply the chain rule on the second term.

$$\begin{aligned}\mathcal{P}(x, A, b) &= x - \eta_v A^\top (Ax - b) \\ \frac{\partial}{\partial x} \mathcal{P}(x, A, b) &= \frac{\partial}{\partial x} (x - \eta_v A^\top (Ax - b)) \\ J_{\mathcal{P}}(x, A, b) &= I_n - \eta_v A^\top A\end{aligned}$$

Both cases are combined in the following matrix formulation with diagonal matrix  $\text{Diag} = \text{diag}((Ax - b)_{>0})$ :

$$J_{\mathcal{P}}(x, A, b) = I_n - \eta_v A^\top \text{Diag} A$$

Finally, we can confirm that Jacobian adjustment is allowed for the unbiased violation projection layer by:

1.  $\mathcal{P}(x, A, b)$  is differentiable as shown above.
2. Due to the full rank nature of the identity  $I_n$  and  $A^\top \text{Diag} A$  when  $\text{Diag} = I_m$ , we get  $\det(J_{\mathcal{P}}(x, A, b)) \neq 0$ , and hence the Jacobian is non-singular.
3.  $\mathcal{P}(x, A, b)$  is locally invertible as  $\det(J_{\mathcal{P}}(x, A, b)) \neq 0$ . It is not globally invertible, due to the piece-wise nature of  $(Ax - b)_{>0}$ .

**Policy Clipping** We can implement a clipped Gaussian distribution that enforces element-wise bounds on a standard Gaussian (Fujita and Maeda 2018). Let  $\mu_\theta$  and  $\sigma_\theta^2$  denote the policy's mean and variance, with bounds  $lb_{pc}$  and  $ub_{pc}$ , and  $\Phi(\cdot)$  being the cumulative distribution function of the standard Gaussian. Actions are sampled from  $\mathcal{N}(\mu_\theta, \sigma_\theta^2)$  and clipping the result to  $[lb_{pc}, ub_{pc}]$ . Provided this transformation, we compute the log probabilities  $\log \pi(x|s)$  for action  $x$  by:

$$\log \pi(x|s) = \begin{cases} \log \Phi \left( \frac{lb_{pc} - \mu_\theta}{\sigma_\theta} \right) & \text{if } x \leq lb_{pc}, \\ -\frac{(x - \mu_\theta)^2}{2\sigma_\theta^2} - \log(\sqrt{2\pi\sigma_\theta^2}) & \text{if } lb_{pc} < x < ub_{pc}, \\ \log \left( 1 - \Phi \left( \frac{ub_{pc} - \mu_\theta}{\sigma_\theta} \right) \right) & \text{if } x \geq ub_{pc} \end{cases}$$

### Unbiased Violation Projection

We define a feasible region of action  $x$  as the polyhedron:

$$PH = \{x \in \mathbb{R}^n : Ax \leq b, x \geq 0\},$$

where  $A \in \mathbb{R}^{m \times n}$  and  $b \in \mathbb{R}^m$ .

Constraints in  $PH$  may be violated during optimization. To quantify these violations, we introduce the violation function:

$$\mathcal{V}(x) = (Ax - b)_{>0},$$

where  $\mathcal{V}(x)_{m_i} > 0$  indicates that constraint  $m_i$  is violated, and  $\mathcal{V}(x)_{m_i} = 0$  means the constraint is satisfied.

**Violation Gradient Descent.** To minimize constraint violations, we update  $x$  for a fixed number of iterations using gradient descent on the violation term  $\|\mathcal{V}(x)\|_2^2$ , which represents the squared distance to feasibility. Differentiating with respect to  $x$ , we derive the update rule:

$$\begin{aligned}x' &= x - \eta_v \nabla_x \|\mathcal{V}(x)\|_2^2 \\ &= x - \eta_v 2A^\top \mathcal{V}(x).\end{aligned}$$

Since the step size  $\eta_v \in (0, 1)$  is a tunable parameter, we simplify the update function to:

$$x' = x - \eta_v A^\top \mathcal{V}(x).$$

**Theorem 1** (Convergence of Violation Gradient Descent). Let  $x_0 \in \mathbb{R}^n$  be an initial point, and consider update:

$$x_{k+1} = x_k - \eta_v A^\top \mathcal{V}(x_k),$$

where:

- $\mathcal{V}(x) = \max(0, Ax - b)$  is the element-wise function onto nonnegative constraint values.
- $\eta_v \in (0, 1)$  is a sufficiently small step size parameter to ensure stable convergence.
- $A \in \mathbb{R}^{m \times n}$  has full row rank.
- The feasible region  $PH = \{x \in \mathbb{R}^n : Ax \leq b, x \geq 0\}$  is nonempty.

Then, the sequence  $\{x_k\}$  satisfies:

1. The function  $g(x) = \|\mathcal{V}(x)\|_2^2$  is non-increasing.
2.  $x_k$  converges to a feasible point  $x^*$  or a local minimum violation point.

*Proof.* Define the violation function:

$$g(x) = \|\mathcal{V}(x)\|_2^2.$$

Since  $\mathcal{V}(x)$  is an elementwise projection onto nonnegative values, and some function  $h(y) = \max(0, y)$  is convex and non-decreasing, then the function  $g(x) = \|\mathcal{V}(x)\|_2^2$  is convex when  $Ax - b$  is affine.

We apply gradient descent on  $g(x)$  using the update rule:

$$x_{k+1} = x_k - \eta_v \nabla_x g(x_k).$$

By the standard descent lemma (Boyd and Vandenberghe 2004), for a sufficiently small step size  $\eta_v$ , we have:

$$g(x_{k+1}) \leq g(x_k) - \eta_v \|\nabla_x g(x_k)\|_2^2.$$

Since  $\eta_v > 0$  and  $\|\nabla_x g(x_k)\|_2^2 \geq 0$ , it follows that:

$$g(x_{k+1}) \leq g(x_k).$$

Thus,  $g(x_k)$  is non-increasing.

Since  $g(x_k)$  is also lower-bounded by 0, it must converge to some limit  $g^* \geq 0$ . This implies:

$$\lim_{k \rightarrow \infty} \|\mathcal{V}(x_k)\|_2 = \tilde{c}, \quad \text{for some } \tilde{c} \geq 0.$$

If  $\tilde{c} = 0$ , then  $x_k$  converges to a feasible point, meaning  $\mathcal{V}(x_k) = 0$ . If  $\tilde{c} > 0$ , then  $x_k$  converges to a local minimum of  $g(x)$ , where no further descent is possible, satisfying  $\nabla_x g(x_k) = 0$ , which implies  $A^\top \mathcal{V}(x_k) = 0$ .  $\square$

## Instance Generator

During training, we simulate problem instances based on a Gaussian distribution with element  $i$ :

$$q^{(i,j,k)} \sim \mathcal{N}(\mu^{(i,j,k)}, \sigma^{(i,j,k)}) \quad \forall (i,j) \in TR, k \in K.$$

Here,  $\mu$  is the expected value of cargo demand, initialized by a uniform generator  $\mathcal{U}(lb, ub)$ , while the standard deviation of demand is defined as  $\sigma^{(i,j,k)} = CV \cdot \mu^{(i,j,k)}$ , where the coefficient of variation (CV) controls the spread of each element based on  $\mu^{(i,j,k)}$ . Note that CV is normally defined as  $CV^{(i,j,k)} = \frac{\sigma^{(i,j,k)}}{\mu^{(i,j,k)}}$ , so we use  $\sigma^{(i,j,k)} = CV \cdot \mu^{(i,j,k)}$  to control the spread of the distribution.

We initialize  $\mu^{(i,j,k)} \sim \mathcal{U}(0, \overline{\mu^{(i,j,k)}})$ , where the upper bound on the expected value is found as follows:

$$\overline{\mu} = \frac{2UR \cdot \mathbf{1}^\top c}{NC},$$

where  $UR$  is the rate of total utilization present in the demand (e.g., 1.2 means total demand is 120% of total capacity), and  $NC \in \mathbb{R}_{>0}^{|TR|}$  is a matrix to spread the demand over different elements proportional to the number of transports remaining to be loaded.

During generalization testing, we simulate problem instances based on a continuous uniform generator:

$$q^{(i,j,k)} \sim \mathcal{U}(lb^{(i,j,k)}, ub^{(i,j,k)}).$$

To ensure similar mean and variance of the instances, we derive parameters  $lb$  and  $ub$  from the definition of the continuous uniform distribution, as follows:

$$\begin{aligned} \mu^{(i,j,k)} &= (lb^{(i,j,k)} + ub^{(i,j,k)})/2 \\ (\sigma^{(i,j,k)})^2 &= (ub^{(i,j,k)} - lb^{(i,j,k)})^2/12 \end{aligned}$$

We rewrite to:

$$\begin{aligned} lb^{(i,j,k)} &= \mu^{(i,j,k)} - \sqrt{(12(\sigma^{(i,j,k)})^2)/2} \\ ub^{(i,j,k)} &= \mu^{(i,j,k)} + \sqrt{(12(\sigma^{(i,j,k)})^2)/2} \end{aligned}$$

## Multi-stage Stochastic MIP

### Multi-stage Scenario Tree

A scenario tree is a directed tree represented as  $T_{ST} = (V_{ST}, E_{ST})$ , where  $V_{ST}$  is the set of nodes, each corresponding to a decision or uncertainty realization at a given stage.  $E_{ST} \subseteq V_{ST} \times V_{ST}$  is the set of directed edges representing transitions between nodes over time.

The tree consists of:

1. A root node  $v_1 \in V_{ST}$ , representing the initial state at the first port.
2. Stages  $p = 1, 2, \dots, N_P - 1$ , where each node  $v$  belongs to a stage  $p(v)$ . We denote stages by  $p$ , as stages are equivalent to ports in a voyage.
3. Branching structure, where each node has child nodes that correspond to possible future realizations.
4. A probability measure  $P_{ST} : V_{ST} \rightarrow [0, 1]$  assigning probabilities to nodes, ensuring:

$$\sum_{v' \in \text{child}(v)} \mathbb{P}(v') = \mathbb{P}(v), \quad \forall v \in V_{ST}.$$

5. Scenario paths  $\phi \in \mathcal{Z}$ , which are root-to-leaf paths representing possible realizations of uncertainty over time.

Intuitively, the scenario tree discretely represents how uncertainty unfolds over time. Each branching point corresponds to a stochastic event, capturing all possible realizations of uncertain parameters across the planning horizon. As we progress through stages, new uncertainty is realized, and decisions are made at each node based on available information. These decisions do not anticipate future realizations, but are optimized over the expected outcomes of all future scenarios encoded in the tree.

## MIP Formulation

We define the MPP under demand uncertainty as a multi-stage stochastic MIP.

**Decision Variables.** The following variables are included:

- Vessel utilization:  $\tilde{u}_{tr,k}^{b,d,\phi} \in \mathbb{Z}_{\geq 0}$
- Hatch overstayage:  $\tilde{ho}_{p,b}^\phi \in \mathbb{Z}_{\geq 0}$
- Makespan of cranes:  $\tilde{cm}_p^\phi \in \mathbb{Z}_{\geq 0}$
- Hatch movement:  $\tilde{hm}_{p,b}^\phi \in \{0, 1\}$

All integer constraints are relaxed linearly in the implementation. Additionally, we use a sufficiently large constant, denoted by big  $M$ , to impose logical constraints as needed.

**Objective.** The objective function (18) maximizes the revenue with parameter  $rev^{(i,j,k)} \in \mathbb{R}_{>0}$  and minimizes hatch-overstowage with parameter  $ct^{ho} \in \mathbb{R}_{>0}$  and crane moves costs with parameter  $ct^{cm} \in \mathbb{R}_{>0}$  over scenario paths  $\phi \in \mathcal{Z}$  each with probability  $\mathbb{P}_\phi$ . We assume each scenario path has equal probability.

**Constraints.** Constraint (19) enforces that the onboard utilization cannot exceed the cargo demand  $q$ , whereas Constraint (20) limits each vessel location to the TEU capacity  $c$  for each bay  $b \in B$  and deck  $d \in D$ . In Constraint (21), we indicate that hatches need to be opened if below deck cargo needs to be loaded or discharged. Based on these movements, Constraint (22) models the amount of hatch overstowage in containers. Subsequently, we compute the target of crane moves  $\bar{z}$  in Constraint (23), after which Constraint (24) computes the excess number of crane moves  $\tilde{cm}$ .

Additionally, we model the longitudinal and vertical stability in Constraints (26) until (29). First, we compute the longitudinal moment, vertical moment and total weight in Constraints (26), (27) and (25), respectively. Second, Constraint (28) bounds  $lcg$  between  $\underline{lcg}$  and  $\overline{lcg}$ . Third, Constraint (29) bounds  $vcg$  between  $\underline{vcg}$  and  $\overline{vcg}$ . Both  $lcg$  and  $vcg$  are linearized equivalents of the original Constraints (1) and (2), respectively. Furthermore, we include non-anticipation in Constraint (30) to prevent leveraging future demand realizations.

$$\max \sum_{\phi \in \mathcal{Z}} \mathbb{P}_\phi \sum_{p \in P} \sum_{b \in B} \sum_{d \in D} \sum_{k \in K} \sum_{tr \in TR^+(p)} rev^{(i,j,k)} \tilde{u}_{tr,k}^{b,d,\phi} - ct^{ho} \tilde{ho}_{p,b}^\phi - ct^{cm} \tilde{cm}_p^\phi \quad (18)$$

$$\text{s.t. } \sum_{b \in B} \sum_{d \in D} \tilde{u}_{tr,k}^{b,d,\phi} \leq q_{tr,k}^\phi \quad \forall p \in P, tr \in TR^{OB}(p), k \in K, \phi \in \mathcal{Z} \quad (19)$$

$$\sum_{k \in K} \sum_{tr \in TR^{OB}(p)} teu_{tr,k} \tilde{u}_{tr,k}^{b,d,\phi} \leq c_{b,d} \quad \forall p \in P, b \in B, d \in D, \phi \in \mathcal{Z} \quad (20)$$

$$\sum_{k \in K} \sum_{tr \in TR^M(p)} \tilde{u}_{tr,k}^{b,d_h,\phi} \leq M \tilde{hm}_{p,b}^\phi \quad \forall p \in P, b \in B, \phi \in \mathcal{Z} \quad (21)$$

$$\sum_{k \in K} \sum_{tr \in TR^{OB}(p)} \tilde{u}_{tr,k}^{b,d_o,\phi} - M(1 - \tilde{hm}_{p,b}^\phi) \leq \tilde{ho}_{p,b}^\phi \quad \forall p \in P, b \in B, \phi \in \mathcal{Z} \quad (22)$$

$$\bar{z}_p^\phi = (1 + \delta^{cm}) \frac{2}{|B|} \sum_{tr \in TR^M(p)} \sum_{k \in K} q_{tr,k}^\phi \quad \forall p \in P, \phi \in \mathcal{Z} \quad (23)$$

$$\sum_{b \in B'} \sum_{d \in D} \sum_{k \in K} \sum_{tr \in TR^M(p)} \tilde{u}_{tr,k}^{b,d,\phi} - \bar{z}_p^\phi \leq \tilde{cm}_p^\phi \quad (24)$$

$$\forall p \in P, b' \in B', \phi \in \mathcal{Z} \quad (24)$$

$$tw_p^\phi = \sum_{k \in K} w_k \sum_{tr \in TR^{OB}(p)} \sum_{d \in D} \sum_{b \in B} \tilde{u}_{tr,k}^{b,d,\phi} \quad \forall p \in P, \phi \in \mathcal{Z} \quad (25)$$

$$lm_p^\phi = \sum_{b \in B} ld_b \sum_{k \in K} w_k \sum_{tr \in TR^{OB}(p)} \sum_{d \in D} \tilde{u}_{tr,k}^{b,d,\phi} \quad \forall p \in P, \phi \in \mathcal{Z} \quad (26)$$

$$vm_p^\phi = \sum_{d \in D} vd_d \sum_{k \in K} w_k \sum_{tr \in TR^{OB}(p)} \sum_{b \in B} \tilde{u}_{tr,k}^{b,d,\phi} \quad \forall p \in P, \phi \in \mathcal{Z} \quad (27)$$

$$\underline{lcgtw}_p^\phi \leq lm_p^\phi \leq \overline{lcgtw}_p^\phi \quad \forall p \in P, \phi \in \mathcal{Z} \quad (28)$$

$$\underline{vcgtw}_p^\phi \leq vm_p^\phi \leq \overline{vcgtw}_p^\phi \quad \forall p \in P, \phi \in \mathcal{Z} \quad (29)$$

$$\tilde{u}_{tr,k}^{b,d,\phi'} = \tilde{u}_{tr,k}^{b,d,\phi} \quad \forall p \in P, tr \in TR^+(p), k \in K, b \in B, d \in D, \phi, \phi' \in \mathcal{Z} \mid q_{[p-1]}^\phi = q_{[p-1]}^{\phi'} \quad (30)$$

## Deep RL Implementation Details

### Feasibility Regularization and Primal-Dual RL

To encourage the policy to produce feasible actions with respect to linear constraints  $A(s_t)x \leq b(s_t)$ , we introduce a soft penalty term into the actor loss:

$$\mathcal{L}(\theta) = -\mathcal{L}_{\text{actor}}(\theta) + \lambda_f \mathcal{L}_{\text{feas}}(\theta), \quad (31)$$

$$\mathcal{L}_{\text{feas}}(\theta) = \mathbb{E}_t [(A(s_t)x_\theta(s_t) - b(s_t))_{>0}], \quad (32)$$

where  $(\cdot)_{>0} = \max(0, \cdot)$  denotes the hinge function penalizing constraint violations. The coefficient  $\lambda_f$  balances reward maximization and constraint satisfaction.

We consider two methods to handle  $\lambda_f$ :

- Static FR fixes  $\lambda_f$  via hyperparameter tuning before training.
- Primal-Dual FR treats  $\lambda_f$  as a dual variable and jointly learns  $\lambda_f$  during training by adding a dual output head to the critic network, updated via gradient ascent to enforce constraints adaptively.

This primal-dual approach alleviates the need for manual tuning and improves constraint satisfaction during training, as demonstrated in Ding et al. (2020).

### PPO Algorithm

PPO is an on-policy reinforcement learning algorithm that seeks to maximize expected cumulative reward while enforcing stable policy updates via clipped importance sampling (Schulman et al. 2017), as outlined in Algorithm 3. The agent collects trajectories, computing  $n_{\text{ppo}}$ -step return to evaluate performance with  $V_\theta(s)$  as estimated state value:

$$G_t^{(n_{\text{ppo}})} = \sum_{k_{\text{ppo}}=0}^{n_{\text{ppo}}-1} \gamma^k r_{t+k_{\text{ppo}}} + \gamma^{n_{\text{ppo}}} V_\theta(s_{t+n_{\text{ppo}}}), \quad (33)$$

To reduce variance, we adopt Generalized Advantage Estimation (GAE) (Schulman et al. 2016):

$$\hat{A}_t^{\text{GAE}} = \sum_{l_{\text{ppo}}=0}^{\infty} (\gamma\lambda)^{l_{\text{ppo}}} \delta_{t+l_{\text{ppo}}}, \quad (34)$$

$$\delta_t = r_t + \gamma V_\theta(s_{t+1}) - V_\theta(s_t). \quad (35)$$

Here,  $\delta_t$  is the temporal difference (TD) residual, which quantifies the advantage of taking action  $x_t$  at state  $s_t$ .

The actor is updated using the PPO clipped surrogate loss:

$$\mathcal{L}_{\text{actor}}(\theta) = \mathbb{E}_t \left[ \min \left( \text{ratio}_t(\theta) \hat{A}_t^{\text{GAE}}, \text{clip}(\text{ratio}_t(\theta), 1 - \epsilon, 1 + \epsilon) \hat{A}_t^{\text{GAE}} \right) \right], \quad (36)$$

where the probability ratio is defined as:

$$\text{ratio}_t(\theta) = \frac{\pi_\theta(x_t|s_t)}{\pi_{\theta_{\text{old}}}(x_t|s_t)}. \quad (37)$$

The critic aims to minimize the squared TD error:

$$\mathcal{L}_{\text{critic}}(\theta) = \mathbb{E}_t \left[ (V_\theta(s_t) - G_t^{(n_{\text{ppo}})})^2 \right]. \quad (38)$$

Finally, the total PPO objective, including feasibility regularization from Equation (32), is given by:

$$\begin{aligned} \mathcal{L}(\theta) = & \mathcal{L}_{\text{actor}}(\theta) + \lambda_c \mathcal{L}_{\text{critic}}(\theta) + \lambda_f \mathcal{L}_{\text{feas}}(\theta) \\ & - \lambda_e \mathbb{E}_t [\text{entropy}(\pi_\theta)], \end{aligned} \quad (39)$$

where  $\lambda_c$ ,  $\lambda_f$ , and  $\lambda_e$  are weighting coefficients for the critic loss, feasibility regularization, and entropy regularization respectively.

---

#### Algorithm 3: Proximal Policy Optimization (PPO)

---

**Require:** Model parameters  $\theta$ , steps  $n$ , learning rate  $\eta$

- 1: **for** each gradient update **do**
- 2:   **for** each step  $t$  **do**
- 3:     Collect  $n$ -step trajectories  $\{(s_t, x_t, r_t, s_{t+1})\}$
- 4:     Compute  $n$ -step returns  $G_t^{(n_{\text{ppo}})}$
- 5:     Compute advantage estimates  $\hat{A}_t^{\text{GAE}}$
- 6:   **end for**
- 7:   Update parameters:  $\theta \leftarrow \theta + \eta \nabla_\theta \mathcal{L}(\theta)$
- 8: **end for**
- 9: **return** Policy  $\pi_\theta$

---

## SAC Algorithm

Soft Actor-Critic (SAC) is an off-policy reinforcement learning algorithm that optimizes both reward maximization and entropy to encourage efficient exploration (Haarnoja et al. 2018), as outlined in Algorithm 4. It is based on maximum entropy reinforcement learning, which aims to learn a stochastic policy that not only maximizes cumulative rewards but also maintains high entropy for robustness and stability. SAC leverages a soft Q-learning approach, using two Q-functions to mitigate overestimation bias, an entropy-regularized policy update, and an automatically adjusted

temperature parameter to balance exploration and exploitation.

The algorithm maintains an actor network for policy learning, two Q-function critics for value estimation, a target Q-network for stable learning, and an adaptive temperature parameter to regulate entropy. The loss functions for standard SAC are derived from the Bellman backup equation and the policy gradient formulation, ensuring convergence to an optimal stochastic policy. We also include feasibility regularization from Equation (32) in the actor loss.

- Compute target Q-value:

$$Q_{\text{target}}(s_t, x_t) = r_t + \gamma \mathbb{E}_{s_{t+1}, x_{t+1} \sim \pi} \left[ \min_{l=1,2} Q_\theta^l(s_{t+1}, x_{t+1}) - \alpha \log \pi_\theta(x_{t+1}|s_{t+1}) \right]$$

- Critic loss:

$$\mathcal{L}_{\text{critic}}(\theta) = \mathbb{E} \left[ (Q_\theta(s_t, x_t) - Q_{\text{target}}(s_t, x_t))^2 \right]$$

- Actor loss:

$$\mathcal{L}_{\text{actor}}(\theta) = \mathbb{E} \left[ \alpha \log \pi_\theta(x_t|s_t) - Q_\theta(s_t, x_t) + \lambda_f \mathcal{L}_{\text{feas}}(\theta) \right]$$

- Temperature loss:

$$\mathcal{L}_\alpha(\theta) = \mathbb{E} \left[ -\alpha (\log \pi_\theta(x_t|s_t) + \text{entropy}_{\text{target}}) \right]$$

This formulation ensures stability and encourages exploration by adapting the trade-off between exploitation and exploration dynamically.

---

#### Algorithm 4: Soft Actor-Critic (SAC)

---

**Require:** Parameters: actor  $\theta_{\text{actor}}$ , critics  $\theta_{\text{critic}}^1, \theta_{\text{critic}}^2$ , targets  $(\theta_{\text{target}}^1, \theta_{\text{target}}^2) = (\theta_{\text{critic}}^1, \theta_{\text{critic}}^2)$ , temperature  $\alpha$ , learning rate actor  $\eta_a$ , learning rate critic  $\eta_c$ , learning rate temperature  $\eta_\alpha$ , soft update parameter  $\tau$ , replay buffer  $\mathcal{D}$ .

- 1: **for** each iteration **do**
- 2:   **for** each environment step  $t$  **do**
- 3:     Sample action  $x_t \sim \pi_\theta(x_t|s_t)$
- 4:     Perform transition  $s_{t+1} \sim \mathcal{T}(s_{t+1}|s_t, x_t)$
- 5:     Observe reward  $r_t = \mathcal{R}(s_t, x_t)$ ,
- 6:     Store  $(s_t, x_t, r_t, s_{t+1})$  in  $\mathcal{D}$ .
- 7:   **end for**
- 8:   **for** each gradient step **do**
- 9:     Sample a minibatch  $(s_t, x_t, r_t, s_{t+1})$  from  $\mathcal{D}$ .
- 10:     Compute target Q-value:  $Q_{\text{target}}(s_t, x_t)$
- 11:     Update parameters:
$$\begin{aligned} \theta_{\text{critic}}^l &\leftarrow \theta_{\text{critic}}^l - \eta_c \nabla_\theta \mathcal{L}_{\text{critic}}(\theta) \text{ for } l \in \{1, 2\} \\ \theta_{\text{actor}} &\leftarrow \theta_{\text{actor}} - \eta_a \nabla_\theta \mathcal{L}_{\text{actor}}(\theta) \\ \alpha &\leftarrow \alpha - \eta_\alpha \nabla_\alpha \mathcal{L}_\alpha(\theta) \\ \theta_{\text{target}}^l &\leftarrow \tau \theta_{\text{critic}}^l + (1 - \tau) \theta_{\text{target}}^l \text{ for } l \in \{1, 2\} \end{aligned}$$
- 12:   **end for**
- 13: **end for**
- 14: **return** Policy  $\pi_\theta$

---

## Hyperparameters

The parameters of the MPP instances, presented in Table 3, are chosen based on domain knowledge to generate problem instances that closely reflect real-world scenarios.

Parameters	Symbol	Value
Voyage length	$N_P$	4
Number of bays	$N_B$	10
Cardinality deck set	$ D $	2
Cardinality cargo set	$ K $	12
Cardinality transport set	$ TR $	6
Vessel TEU	$\mathbf{1}^\top c$	1,000
Long term contract reduction	$LR$	0.3
Utilization rate demand	$UR$	1.1
lcg bounds	$(\underline{lcg}, \overline{lcg})$	(0.85,1.05)
vcg bounds	$(\underline{vcg}, \overline{vcg})$	(0.95,1.15)
Crane moves allowance	$\delta^{cm}$	0.25
Overstowage costs	$ct^{ho}$	0.33
Crane move costs	$ct^{ho}$	0.5

Table 3: Instance parameters.

Table 4 provides the hyperparameters of projected and vanilla PPO and SAC. Hyperparameter tuning is performed using Bayesian optimization via the Weights & Biases platform (Biewald 2020). Only a selected subset of hyperparameters are optimized, each bounded by specified minimum and maximum values in Table 4. The tuning process uses the objective value as the primary selection criterion, prioritizing feasible solutions whenever possible.

## Additional Experiments

In Table 5, we analyze the vanilla AM policy with feasibility regularization (FR) with static Lagrangian multipliers ( $\lambda_f$ ), and primal-dual methods (PD) that learn the Lagrangian multipliers ( $\lambda_f$ ). We show the performance learned through SAC and PPO, and also show how post-hoc feasibility recovery (FR+R, PD+R) impacts the objective value.

Settings		Projection Algorithms		Vanilla Algorithms		Ranges	
Hyperparameters	Symbol	PPO	SAC	PPO	SAC	Min	Max
<b>Actor Network</b>		Attention	Attention	Attention	Attention	4	16
<b>Number of Heads</b>		8	8	4	4	4	16
<b>Hidden Layer Size</b>		128	128	256	256	128	512
<b>Encoder Layers</b>		3	3	2	1	1	3
<b>Decoder Layers</b>		3	3	3	3	1	3
<b>Critic Network</b>		$1 \times \text{MLP}$	$2 \times \text{MLP}$	$1 \times \text{MLP}$	$2 \times \text{MLP}$		
<b>Critic Layers</b>		4	4	4	4	2	4
<b>Target Network</b>		No	Soft Update	No	Soft Update		
<b>Target Update Rate</b>	$\tau$	N/A	0.005	N/A	0.005		
<b>Dropout Rate</b>		0.009	0.009	0.073	0.164	0.001	0.2
<b>Max Policy Std.</b>		1.931	1.931	1.118	1.779	0.01	10.0
<b>Optimizer</b>		Adam	Adam	Adam	Adam		
<b>Learning Rate (LR)</b>	$\eta$	$1.47 \times 10^{-4}$	$1.47 \times 10^{-4}$	$9.64 \times 10^{-4}$	$9.10 \times 10^{-4}$	$1.0 \times 10^{-6}$	0.01
<b>Primal-Dual LR</b>	$\eta_{pd}$	-	-	$3.47 \times 10^{-5}$	$3.47 \times 10^{-5}$	$1.0 \times 10^{-6}$	0.01
<b>Batch Size</b>		64	64	64	64	16	512
<b>Embedding Size</b>		128	128	128	128	64	256
<b>Discount Factor</b>	$\gamma$	0.99	0.99	0.99	0.99		
<b>GAE</b>	$\lambda$	0.95	N/A	0.95	N/A		
<b>Value Coefficient</b>	$\lambda_c$	0.50	N/A	0.50	N/A		
<b>Entropy Coefficient</b>	$\lambda_e$	0.010	Learned	0.061	Learned		
<b>Feasibility Penalty</b>	$\lambda_f$	Vector	Vector	Vector	Vector	0.01	10.0
<b>Clip Parameter</b>	$\epsilon$	0.2	N/A	0.2	N/A		
<b>Replay Buffer</b>		No	Yes	No	Yes		
<b>Replay Buffer Size</b>		N/A	$10^4$	N/A	$10^4$		
<b>Mini-batch Size</b>		32	32	32	32	16	64
<b>Update Epochs</b>		5	1	5	1	3	20
<b>Entropy Target</b>		N/A	$- X $	N/A	$- X $		
<b>Projection LR</b>	$\eta_v$	0.01	0.01	N/A	N/A	0.001	0.1
<b>Projection Epochs</b>		300	300	N/A	N/A	50	500
<b>Inference Threshold</b>	$\delta_v$	0.01	0.01	N/A	N/A	0.001	0.1
<b>Training Budget</b>		$7.2 \times 10^7$	$7.2 \times 10^7$	$7.2 \times 10^7$	$7.2 \times 10^7$		
<b>Validation Budget</b>		$5.0 \times 10^3$	$5.0 \times 10^3$	$5.0 \times 10^3$	$5.0 \times 10^3$		
<b>Validation Frequency</b>		Every 20%	Every 20%	Every 20%	Every 20%		

Table 4: Comparison of hyperparameters for projected and vanilla PPO and SAC.

Methods			Testing ( $N = 30$ )		
Alg.	Model	F.M.	Obj. (\$)	Feas. (%)	$d(\mathbf{PH}(s_t))$
SAC	AM	FR	1,188.90	0.00	83.03
SAC	AM	FR+R	1,217.22	100.00	0.00
SAC	AM	PD	1,077.84	0.00	30.21
SAC	AM	PD+R	1,080.21	100.00	0.00
PPO	AM	FR	1,294.31	0.00	2,565.51
PPO	AM	FR+R	1,133.18	100.00	0.00
PPO	AM	PD	1,149.44	0.00	1,441.97
PPO	AM	PD+R	885.85	100.00	0.00

Table 5: Performance on  $N$  instances of feasibility regularization (FR), primal-dual methods (PD), and their feasibility-recovered variants (FR+R, PD+R). Metrics include average objective profit (Obj.), inference time (Time), feasibility rate (Feas.), and total absolute distance to the feasible region  $d(\mathbf{PH}(s_t))$ .